REPORT DOCUMENTATION PAGE

Form Approved
OMB NO. 0704-0188

1. AGENCY USE ONLY (Leave Blank)	2. REPORT DATE	3. REPORT TYPE AND DATES COVERED
	12-09-98	Final. 04-15-95 to 01-14-99

4. TITLE AND SUBTITLE
Rheological properties of low density snow

5. FUNDING NUMBERS
DAAH04-95-1-0172

6. AUTHOR(S)
Howard Conway

7. PERFORMING ORGANIZATION NAME(S) AND ADDRESS(ES)
University of Washington
Geophysics, Box 351650
Seattle, WA 98195-1650

8. PERFORMING ORGANIZATION REPORT NUMBER
PR-4

9. SPONSORING / MONITORING AGENCY NAME(S) AND ADDRESS(ES)
U. S. Army Research Office
P.O. Box 12211
Research Triangle Park, NC 27709-2211

10. SPONSORING / MONITORING AGENCY REPORT NUMBER
ARO 33797.5-EV

11. SUPPLEMENTARY NOTES
The views, opinions and/or findings contained in this report are those of the author(s) and should not be construed as an official Department of the Army position, policy or decision, unless so designated by the documentation.

12 a. DISTRIBUTION / AVAILABILITY STATEMENT
Approved for public release; distribution unlimited.

12 b. DISTRIBUTION CODE

13. ABSTRACT (Maximum 200 words)
Widespread slab avalanches up to 1m deep often release immediately after the onset of rain on new snow. Measurements show that on first wetting the densification rate increases by about three orders of magnitude. It is likely that the initial burst of densification is a result of rapid structural changes and grain rearrangement. Abrupt changes in the mechanical properties are also likely but measurements show that only the upper 0.15m or less of the snowpack has been affected at the time of avalanching. We have not detected changes at the sliding layer. Results from an elastic slip-weakening model show the slab modulus may have a controlling influence on slope stability. It is evident that the mechanical properties of both the weak layer and the slab control slope stability. We have investigated the evolution of snow slope stability during storms by tracking the shear strength at a potential weak layer and the shear stress imposed by the weight of the overburden. Preliminary tests with the model are promising and State highway avalanche technicians plan to use it operationally at Snoqualmie Pass in the Washington Cascades during the coming winter.

14. SUBJECT TERMS	15. NUMBER OF PAGES
Snow, rain-on-snow, rheology, avalanches	27
	16. PRICE CODE

17. SECURITY CLASSIFICATION OF REPORT	18. SECURITY CLASSIFICATION ON THIS PAGE	19. SECURITY CLASSIFICATION OF ABSTRACT	20. LIMITATION OF ABSTRACT
UNCLASSIFIED	UNCLASSIFIED	UNCLASSIFIED	UL

RHEOLOGICAL PROPERTIES OF LOW DENSITY SNOW

Final Progress Report

by

HOWARD CONWAY

December 9, 1998

U.S. ARMY RESEARCH OFFICE

DAAH04-95-1-0172

UNIVERSITY OF WASHINGTON

Approved for public release;

Distribution unlimited.

TABLE OF CONTENTS

1. PROBLEM STATEMENT

Progress in solving practical problems such as calculating the load-bearing capacity for vehicles, calculating stresses imposed by snow on structures, and predicting avalanche release has been hampered because of lack of knowledge of the mechanical properties of snow. The problem is particularly complex because the properties of natural snowpacks vary both spatially and temporally and this often has a controlling effect on the bulk behavior. For example it is thought that snow slope stability is controlled by rather small-scale (~ 1 to 10m) flaws buried within the snowpack (*McClung, 1979; Conway and Abrahamson 1984; Schweizer, 1998*). Further, the spatial pattern might evolve rapidly over time. For example observations indicate slope stability often changes immediately following the onset of rain (*Conway and Raymond, 1993*), probably in response to rapid changes in the mechanical properties that occur when snow becomes wet (*Conway, 1998; Marshall et al., 1998*).

It is well known that the mechanical properties of snow depend on microstructure (*e.g., Kry, 1975; Hansen and Brown, 1987; Edens and Brown, 1991; Mahajan and Brown, 1993*) but the relevant microstructural properties are generally not known nor measured. Here we have examined the mechanical behavior of snow using both theory and measurements with the idea of parameterizing mechanical properties using commonly measured variables. We acknowledge that this semi-empirical approach has limitations, but our work is motivated by the need for solutions to practical problems.

An important finding has been the importance of metamorphic processes which cause changes independently of gravitational stresses. These are particularly evident during wetting of new snow when metamorphic processes may cause properties to change several orders of magnitude within a few minutes. We have also studied both the consequences of rain on snow slope stability, and the evolution of slope stability during storms. Results, summarised below, are also given in manuscripts that are either published or submitted for publication. These are attached as appendixes.

2. SUMMARY OF IMPORTANT RESULTS

2.1 Snow densification during wetting

Experiments designed to examine the effects of wetting show that the densification rate of low density snow typically increases by three orders of magnitude during first wetting. This is much faster than previously thought. The initial burst of densification occurs independently of gravitational loading and is probably a result of the rapid structural changes that occur during first wetting. We choose to model the process by modifying a standard linear viscous constitutive relationship (eg. *Kojima, 1967*) often used for snow, with a time-dependent metamorphic component. We assume the metamorphic component is additive to the stress component and in this way retain the tractability of the constitutive approach. Details are given in our manuscript *Snow densification during rain*. The model fits measurements very well, although we caution that more experiments are need to determine the dependence of model parameters on liquid water content. The validity of any empirical model becomes suspect when extrapolating beyond the range of experimental conditions from which it was derived.

Nevertheless the experiments have quantified the rapid changes in deformational behavior when snow is first wetted, and have yielded new insight into processes that might control snow slope stability at the onset of rain. These are discussed in more detail below.

2.2 Slope stability at the onset of rain

Slab avalanche activity is often immediate and widespread immediately after the onset of rain-on-snow (*Conway and Raymond, 1993*). This realization has improved predictions of the release of this type of avalanche; prediction relies on accurately forecasting the time snowfall will change to rain. This is possible using measurements telemetered from automatic weather stations that are located at remote sites near the avalanche start zones.

However the mechanism of release has been a puzzle for many years because the rate of infiltration of liquid water and the associated thermal wave has been shown to be too slow to significantly affect the strength of the sliding layer by the time the avalanches release (*Conway and Raymond, 1993*). Our more extensive measurements of temperature and creep profiles made at high spatial and temporal resolution in natural snow confirm that the rain does not affect the sliding layer directly. We have used an elastic slip-weakening model (*McClung, 1979*) to study conditions in a snowpack at the onset of rain. Details are given in our manuscript *The impact of surface pertubations on snow slope stability*. Results show that alteration of the surface properties can *soften* the slab (the effective slab modulus is reduced) and the associated release of strain energy propagates rapidly to the weak layer.

This finding is particularly important because it indicates that snow slope stability depends on the mechanical properties of both the weak layer and the overlying slab. Field practioners generally focus attention on the weak layer but in some cases the the slab properties might control slope stability. Because avalanching is so widespread, and the perturbation from the rain is relatively small, a further implication is that the stability of freshly deposited snow must often be close to critical. The analysis reinforces the idea that freshly deposited snow on slopes should be treated with caution.

2.3 Slope stability during storms

The goal of this work is to find a way to predict snow slope stability using commonly measured meteorological and snowpack variables (accumulation rate, temperature and snow density). The work is motivated by the need to improve operational avalanche forecasting during storms. This is particularly relevant for ski area and highway operations which require rapid evaluations of slope stability over wide areas.

We assume a slope will become unstable when the shear strength of a layer buried at depth is exceeded by the shear stress imposed by the weight of the overburden. This assumption neglects any contribution from longitudinal stresses in the slab (discussed in the previous section) and so is expected to provide a conservative estimate of the onset of instability. The evolution of shear stress on a slope of given angle can be calculated directly from measurements of precipitation. We parameterize the shear strength as a power-law function of snow density (*Gibson and Ashby, 1987*). Although the parameterization is not perfect, given other uncertainties it appears to be adequate for the range of densities and strengths that control snow slope stability (low density, weak snow). The initial density of the new snow is estimated from measurements of air temperature and wind speed, and the evolution of density is modeled using a viscous constitutive law. The density (and hence the strength) of a snow layer generally increases both with time, and as the load from the overburden increases. There is a competition between the rate of loading from the new snow and the rate of strengthening of the buried layer.

Details of the model are given in our manuscript *Evolution of snow slope stability during storms*. Analysis of the errors indicates that most of the model uncertainty stems from the estimate of the initial snow density and we are hoping to improve this parameterization in the near future. Preliminary results are very encouraging. We have tested the model using measurements from three storm cycles at Snoqualmie Pass in the Washington Cascades. We have just installed the model for operational use by Washington State avalanche technicians at Snoqualmie Pass on the I-90 corridor.

3. LIST OF PUBLICATIONS (copies of manuscripts are attached in appendix)

Conway, H., S. Breyfogle, J.B. Johnson and C.Wilbour, 1996. Creep and failure of alpine snow: Measurements and observations. *Proceedings, Int. Snow Science Workshop held in October 1996 at Banff, Alberta, 107-112.*

Conway, H., 1998. The impact of surface perturbations on snow slope stability. *Annals Glaciology, 26, 307-312.*

Marshall, H.-P., H. Conway and L.A. Rasmussen. Snow densification during rain. *(Presented at Int. Snow Science Workshop, held in October 1998 at Sunriver, Oregon and submitted to Cold Regions Science and Technology).*

Conway, H. and C. Wilbour. Evolution of snow slope stability during storms. *(Presented at Int. Snow Science Workshop, held in October 1998 at Sunriver, Oregon and submitted to Cold Regions Science and Technology).*

4. SCIENTIFIC PERSONNEL SUPPORTED BY THE PROJECT

Howard Conway
Hans-Peter Marshall
- NASA Space Grant Scholarship, 1997
- NASA Space Grant scholarship, 1998
- Bonderman Honors travel fellowship, 1998
- Mary Gates Honours scholarship, 1998
- BS (physics and geophysics), expected in spring 1998

Al Rasmussen
Tim Schaub
Steve Breyfogle

5. BIBLIOGRAPHY

Conway, H. and J. Abrahamson, 1984. Snow stability index. *J. Glaciol.*, 30 (106), 321-327.

Conway, H. and C.F. Raymond, 1993. Snow stability during rain. *J. Glaciol.*, 39 (133), 635-642.

Conway, H., 1998. The impact of surface perturbations on snow slope stability. *Annals. Glaciol.*, 26, 307-312.

Gibson, L.J. and M.F. Ashby, 1987. *Cellular solids. Structure and properties.* Pergamon Press, New York.

Edens, M.Q. and R.L. Brown, 1991. Changes in microstructure of snow under large deformations. *J. Glaciol.*, 37 (126), 193-202.

Hansen, A.C. and R.L. Brown, 1987. A new constitutive theory for snow based on a micromechanical approach. *IAHS Pub. No. 162, 87-104.*

Kojima, K. 1967. Densification of seasonal snowcover. In Physics of Snow and Ice, *Proceedings Int. Conf. on Low Temp. Sci. Hokkaido University, Sapporo, Japan, edited by H. Oura*, Vol. 1, 929-952.

Kry, P.R. 1975. Quantitative stereological analysis of grain bonds in snow. *J. Glaciol., 14(72), 467-477.*

Mahajan, P. and R.L. Brown, 1993. A microstructure-based constitutive law for snow. *Annals Glaciol.* 18, 287-294.

McClung, D.M. 1979. Shear fracture precipitated by strain softening as a mechanism of dry slab release. *J. Geophys. Res., 84(B7),* 3519-3526.

Schweizer, J. 1998. On the role of deficit zones or imperfections in dry snow slab avalanche release. *Proceedings, Int. Snow Science Workshop, Sunriver, Oregon.*

Annals of Glaciology 26 1998

The impact of surface perturbations on snow-slope stability

H. Conway
Department of Geophysics, University of Washington, Box 351650, Seattle, WA 98195, U.S.A.

ABSTRACT. Measurements and observations by others indicate that a potential slab avalanche consists of a relatively cohesive slab of snow overlying a thin weak layer that contains flaws where locally the shear stress from the overburden is not fully supported. Under favorable conditions, snow will shear strain-soften, which provides the basis for applying a slip-weakening model to examine the size of flaw needed to initiate sub-critical crack propagation along the weak layer. Using typical values for snow properties, the model predicts sub-critical crack growth can initiate from a relatively small flaw well before the shear stress from the overburden approaches the peak shear strength at the bed. The occurrence of small flaws or imperfections in the basal layer would explain field measurements which usually indicate that avalanching occurs before the applied shear stress exceeds the shear strength at the basal layer.

Widespread slab-avalanche activity often increases significantly soon after the onset of rain on new snow. Measurements of temperature and mechanical properties show that only the upper 0.15 m or less of the slab has been altered at the time of avalanching; alterations at the sliding layer have not yet been detected. Results from the slip-weakening model indicate that the rain-induced alterations would reduce the size of flaw needed to initiate sub-critical crack growth by 10–20%. The observations and model results show clearly the importance of the slab properties; it is evident that both the slab and the weak layer act together to control slope stability. A further implication is that the stability of freshly deposited snow is often close to critical, because a relatively small surface perturbation is often sufficient to cause avalanching. This is not surprising, because it is well known from field observations that new snow on slopes should be treated with caution.

BACKGROUND

Widespread avalanche activity often increases significantly a few minutes after the onset of rain on freshly deposited snow. These avalanches usually release as slabs several hours before liquid water and the associated thermal wave has penetrated to the sliding layer (Conway and Raymond, 1993). The abrupt change in stability following relatively small alterations that are restricted to the surface has been a puzzle. The failure layer is dry at the time of avalanching and it is unlikely that the increased avalanche activity is caused simply by the additional gravitational loading associated with the rainfall, because continued loading at the same rate but from snowfall does not usually cause such widespread and immediate avalanching. Apparently, snowpacks just prior to rain often exist in a metastable condition and perturbations caused by the rain are sufficient to alter slope stability. Here, I present and discuss measured changes of mechanical and thermal properties at the onset of rain in the context of the observed rapid and widespread avalanche activity. I make use of an existing model of dry snow-slab failure to examine the impact of rain-induced alterations and use the results to infer pre-failure conditions in the snowpack.

FIELD MEASUREMENTS

The study site is in the Cascade mountains near Snoqualmie Pass, Washington, U.S.A. where mid-winter rain on snow is common. In collaboration with avalanche technicians from the Washington State Department of Transportation, we have contiguous measurements of weather conditions (winds, air temperature and precipitation) and snow properties (layer stratigraphy, temperature and creep profiles). Some measurements are discussed below.

In-situ measurements of creep and temperature

Figure 1a shows the set-up used to measure creep and temperature profiles on slopes. Shoes made from light-weight aluminium screening were placed sequentially at the surface after accumulations of 0.1–0.3 m of snow. The vertical velocity profile was obtained by measuring the position of shoes that were constrained to slide down a fixed pole. A sliding contact mounted on each shoe made electrical contact with a resistance wire attached to the pole and time variations of the vertical position of each shoe were calculated from this voltage-divider circuit. Calibrated thermistors attached to the shoes were used to obtain temperature profiles. The non-vertical component of motion was measured by running a cord from a second shoe up-slope to a rotary potentiometer mounted on the vertical velocity shoe. Initially, the distance between pairs of shoes was set at about 1 m. Measurements were multiplexed and recorded at 5 minute intervals using a data logger and storage module. Shoe positions could be resolved with an accuracy of about ± 2 mm; temperatures were accurate to $\pm 0.01\,^{\circ}$C. The measurements were made near the middle of a 200 m long slope inclined at an angle of 36°. No avalanches released on the study slope while it was instrumented.

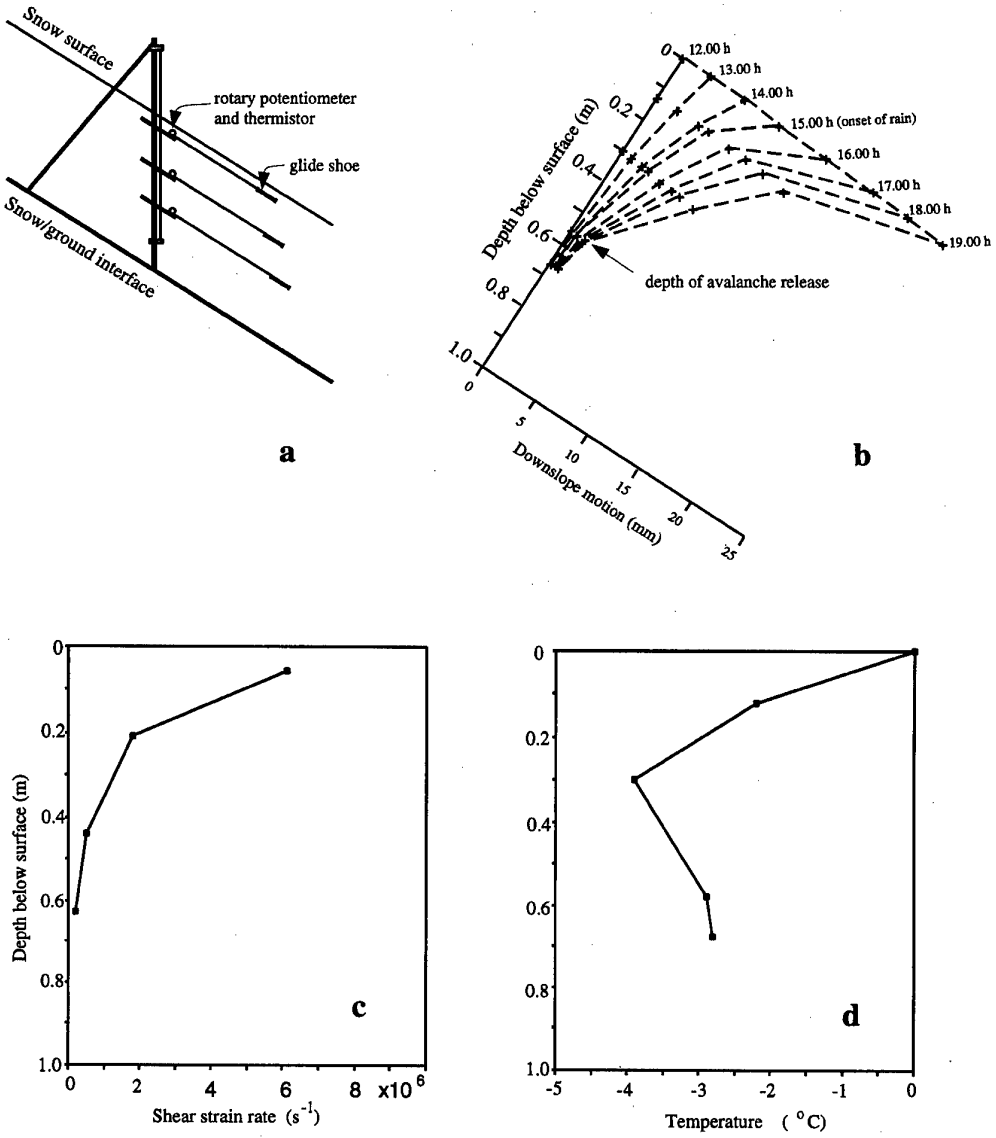

Fig. 1. (a) Experimental set-up used to measure creep and temperature profiles on slopes. (b) shows an example of creep profiles at 1 hour intervals starting at midday on 24 January 1993. Rain started at 15.00 h and many slab avalanches 0.55 m deep released on surrounding slopes soon after the rain started. (c) and (d) show shear strain-rate and temperature profiles 15 minutes after the rain started.

Figure 1b shows a typical example of creep measurements before and after a major rain-on-snow avalanche cycle. The material lines are drawn at hourly intervals and show the evolution of creep before and after rain which started at the site at 15.00 h on 24 January 1993. Rain, first on 22 December 1992 and again on 3 January caused the snow deeper than 0.55 m to settle and become relatively homogeneous. Snow, starting on 20 January, fell on a thin layer of faceted crystals. On steeper slopes, several slab avalanches released at the faceted layer early in the storm but activity increased significantly and many slabs about 0.55 m deep released on all slopes soon after the onset of rain. Measurements show that most of the curvature in the creep profile was caused by differences in the rate of (vertical) settlement through the snowpack. The rate of motion decreased rapidly with density and large gradients in the velocity profile occurred because of contrasts in layer properties. Figure 1c and 1d show respectively the shear strain-rate and the temperature profile during the first 15 minutes following the onset of rain. Field observations of avalanche activity indicated that most slopes had avalanched by this time. During this first 15 minutes, the near-surface strain-rate was more than three times higher than that at depth (Fig. 1c) and only the surface snow had warmed to 0°C (Fig. 1d). The finite vertical spacing between the glide shoes and thermistors made it difficult to resolve all details of the profiles. It is likely that local strain rates were higher than those averaged values and that liquid water and the associated thermal wave had penetrated beneath the surface (although less than 0.12 m) at the time of avalanching.

This response to the first warming or wetting of freshly deposited snow is typical. On horizontal snowpacks, we have measured similar rates of penetration of liquid water and the thermal wave (Conway and Benedict, 1994), and similar compactive strain-rate profiles (Conway and Raymond, 1993). In addition, our stratigraphic measurements from snow pits soon after the onset of rain almost always show liquid water is contained within the upper 0.15 m of the snowpack. The degeneration of mechanical properties such as elastic modulus and fracture toughness with the

introduction of liquid water is not surprising and the abrupt change in stability at the onset of rain is likely a response to both changes in the mechanical properties at the surface and additional loading from the rain. Below, I use existing models of snow properties and slope stability to evaluate the impact of these alterations.

SNOW-SLOPE FAILURE

Stratigraphic observations and measurements at slab-avalanche fracture lines generally show a relatively thick cohesive layer of snow overlying a much thinner weak layer. Experimental evidence from McClung (1977) shows that snow will strain-soften under favorable conditions of rapid shear deformation, which makes it appropriate to analyze conditions in terms of slip-weakening models in which the shear strength in a crack-like weak layer degrades with ongoing slip. Such models have been used successfully to describe instabilities along crustal faults caused by earthquakes (e.g. Li, 1987).

This approach was taken by McClung (1979, 1981), who studied two extreme cases for dry-slab failure: (1) the case where the applied shear stress was sufficient to cause a large area of the weak basal layer to soften, resulting in a dynamic propagating instability. These conditions might be expected during continued natural loading by snowfall. Rapid failure is expected as the applied shear stress approaches the peak strength of a thin, strain-softening basal layer (McClung, 1979, 1981). (2) the case where slip within the basal layer was non-uniform and stress concentrations acting at the edges of a small locally failed zone caused it to expand slowly until the limiting conditions for rapid shear failure were met. In Nature, variations in both the driving stress (from changes in the slab thickness and/or density) and the resistance (from rather small changes in the structure and/or stratigraphy at the basal layer) could initiate non-uniform slip at the bed (Conway and Abrahamson, 1984). Of course, the temporal evolution of the strength of the basal layer as a result of sintering or recrystallization of grains also has important controls on slope stability but that is beyond the scope of this paper.

McClung's (case 2) analysis was based on a slip-weakening model from Palmer and Rice (1973), who showed that shear propagation of crack-like surfaces could be analyzed using an energy criterion. Figure 2 shows a schematic view of a slab overlying a zone of length $2L$ where the shear stress from the overburden is not fully supported. Propagation will occur if the energy released as the slab moves downslope exceeds the energy necessary for plastic yielding at the crack tip. During deformation, under a gravitational shear stress τ_g, the peak shear stress τ_p decreases to a residual τ_r after a characteristic distance δ. The propagation condition for a linear-elastic slab overlying a slip-weakening layer is (McClung, 1979, 1981):

$$\frac{H}{2E}\left[(\tau_g - \tau_r)\frac{L}{H}\right]^2 > (\tau_p - \tau_r)\delta \qquad (1)$$

where E is the average elastic (or viscoelastic modulus) of a slab of thickness H. Laboratory-scale experiments by McClung (1977) indicated $\delta \sim 2$ mm, and $\tau_r/\tau_p \sim 0.75$, although others have reported values for τ_r/τ_p as low as 0.1 (de Montmollin, 1982; Perla and others, 1982). Model assumptions require L to be larger than the end-zone, where the distribution of stresses through the slab is not linear. Physically, this length is expected to be several slab thicknesses. Following from case 1, immediate crack propagation is expected if τ_g exceeds τ_p.

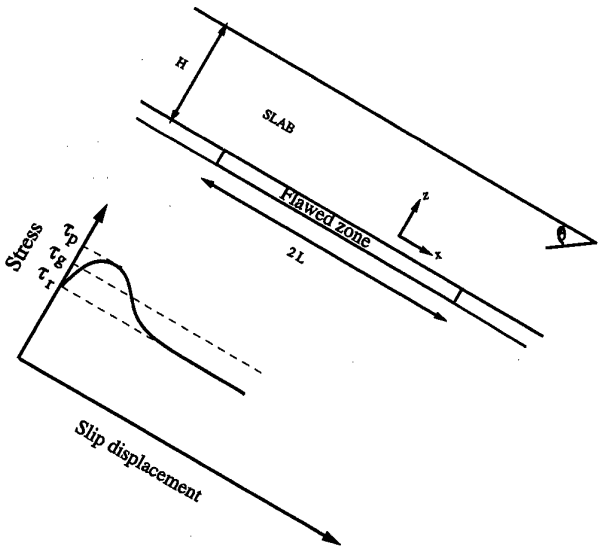

Fig. 2. Schematic of a snow slab overlying a weak layer that contains a flaw (where the gravitational shear stress τ_g is not fully supported) of length 2L. The lower plot shows a weak layer with a peak shear strength τ_p, that slip-weakens to a residual strength τ_r.

The mechanical properties of snow depend strongly on microstructure (Kry, 1975), but the relevant microstructural properties are not generally known nor measured. Although not ideal, bulk density is more easily (and more often) measured and offers a practical alternative. Both snow strength and ductility increase rapidly with density and experiments show a power-law relationship explains much of the variability in measurements of shear strength (Perla and others, 1982; Jamieson, 1995):

$$\tau_p = C(\rho_s/\rho_i)^2 \qquad (2)$$

where τ_p is the peak shear strength (in Pa), ρ_s is the snow density and ρ_i is the density of ice (917 kg m^{-3}). The coefficient C depends on grain structure and varies from 1.8×10^4 Pa for open-grain structures (such as faceted grains) to 2.2×10^4 Pa for partly metamorphosed new snow.

For dry low-density snow (<400 kg m^{-3}), the elastic modulus E (in Pa) is also conveniently described by a power-law relationship (Gibson and Ashby, 1987; Mellor, 1977):

$$E = 2.2 \times 10^7 \, (\rho_s/\rho_i)^2 . \qquad (3)$$

The average modulus for a layered slab can be approximated as:

$$E_{avg} = \frac{E_1H_1 + E_2H_2 + \ldots}{H_1 + H_2 + \ldots} \qquad (4)$$

where E_1, E_2, etc. are the values of the modulus of layers of thickness H_1, H_2, etc.

Numerical examples

Equation (1) implies sub-critical crack growth will occur only when the flaw or imperfection exceeds a certain length. For practical purposes, it is of interest to determine the mini-

mum flaw size needed to initiate slow-failure propagation. The size depends on the mechanical properties of the system and it is convenient to study the length as a function of τ_p/τ_g because rearrangement of Equation (1) shows this relationship is relatively insensitive to changes in slope angle, slab thickness and density of both the slab and the weak layer. I restricted the analysis to flaws with a half-length less than 10 m, because rapid dynamic failure was expected if the "flaw" extended over a large area.

Values for the mechanical properties were estimated using Equations (2) and (3) for a range of conditions typically observed at avalanche-fracture lines (e.g. McClung and Schaerer, 1993). The gravitational shear stress τ_g was assumed constant and failure initiated from a flaw (of half length L), where the basal shear strength τ_r was less than τ_g. For simplicity, I assumed the residual strength of the basal layer (after shear-strain softening) was also τ_r and used the slip-weakening model (Equation (1)) to examine the sensitivity of L to changes in properties of the slab and the weak layer.

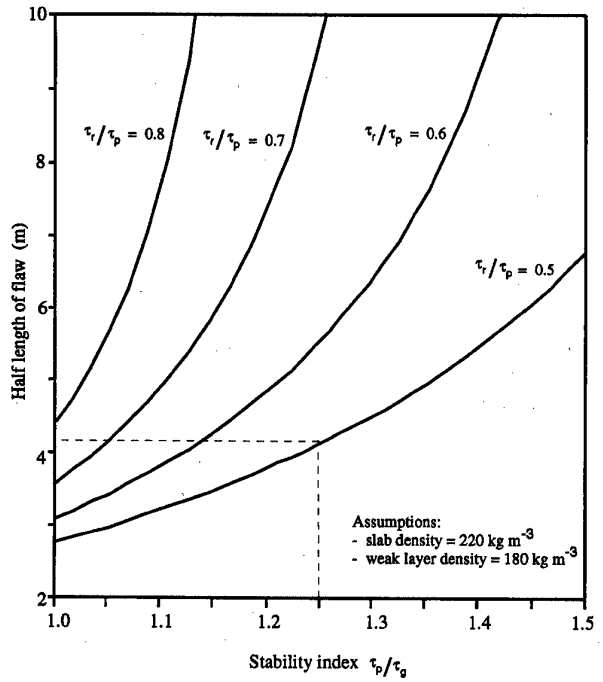

Fig. 3. Half-length of flaw needed to cause sub-critical crack growth as a function of the stability index τ_p/τ_g and the strain-softening ratio τ_r/τ_p. Results show sub-critical crack growth can initiate from relatively small flaws well before the average stability index decreases to 1.0. The example shows (for $\tau_p/\tau_g = 1.25$) a flaw of half-length 4.2 m will propagate when $\tau_r/\tau_p = 0.5$ but the half-length necessary for propagation increases (unrealistically) to more than 400 m when $\tau_r/\tau_p = 0.8$.

Results, together with values used for model input, are shown in Figure 3. τ_p/τ_g has been called "the stability index" by several authors; failure is expected to be immediate (i.e. $L = 0$) when the stability index is 1.0. The model discrepancy (shown in Figure 3 when $\tau_p/\tau_g = 1$) arises because of end-zone effects discussed earlier. Nevertheless, results show clearly that the length of the flaw needed to cause sub-critical crack growth decreases rapidly as τ_p/τ_g decreases. Indeed, the length decreases by about 50% when τ_p/τ_g decreases by only 10%. Changes of this magnitude could arise if either the slope angle, slab density, slab thickness or weak-layer density changed by just 5–10%, which is well within the bounds of natural variability measured across slopes. This sensitivity contributes to making accurate field assessment of slope stability problematic.

Results shown in Figure 3 also indicate the flaw length is highly sensitive to the residual strength. Reducing the residual strength allows initiation of sub-critical crack growth from relatively small flaws well before the average stability index for the slope becomes unity. Figure 3 shows (for $\tau_p/\tau_g = 1.25$) a flaw with a half length of just 4.2 m will result in sub-critical crack growth when $\tau_r/\tau_p = 0.5$, but the length increases rapidly to more than 400 m when $\tau_r/\tau_p = 0.8$. (Such a long length is unrealistic, because the zone is no longer a "flaw".) The idea that widespread slope failure can initiate from a relatively small flaw is supported by measurements which show the average stability index for avalanched slopes is usually greater than 1.0 (Jamieson, 1985).

Uncertainties in the spatial and temporal distribution of snow properties and flaws make it difficult to predict snow-slope stability accurately. However, the abrupt change in stability at the onset of rain offers some clues about conditions in the snowpack prior to rain and this is considered in the next section.

Avalanching at the onset of rain

Observations suggest that new snow often exists in a metastable condition and small perturbations at the onset of rain cause abrupt and widespread avalanching. McClung (1996) showed that the elastic modulus is highly temperature sensitive and experimental evidence indicates it is often reduced by an order of magnitude with the introduction of liquid water. The elastic energy released by the slab following an abrupt decrease in the slab modulus would would be available to drive crack propagation (Equation (1)). Assuming the modulus prior to rain E_0 is constant through the slab of thickness H_0, using Equation (4) the average modulus after rain E_1 can be written:

$$E_1 = \frac{E_s H_s + E_0(H_0 - H_s)}{H_0} \qquad (5)$$

where E_s is the modulus of the wetted surface layer of thickness H_s. Generally, $E_s H_s \ll E_0(H_0 - H_s)$ and a reasonable approximation for the slab-averaged modulus is:

$$E_1 = \frac{E_0(H_0 - H_s)}{H_0}. \qquad (6)$$

Here, $H_0 - H_s$ can be considered to be the "effective" slab thickness after wetting. Assuming τ_p, τ_r and δ do not change in the first few minutes following the onset of rain but allowing that additional loading from rain may increase the basal shear stress to τ_{g1}, re-arrangement of Equation (1) yields

$$\frac{L_0}{L_1} > \sqrt{\frac{H_0}{(H_0 - H_s)}\,\frac{(\tau_{g1} - \tau_r)}{(\tau_{g0} - \tau_r)}}. \qquad (7)$$

Measurements of creep and temperature discussed above indicate that liquid water and the associated alteration of the mechanical properties are usually limited to the upper 0.1–0.15 m during the first 15 minutes of rain. Typical rates of precipitation in the region (5–10 mm h^{-1}) would increase the gravitational shear stress by about 30–60 Pa h^{-1} on a slope

of angle 38°. Figure 4 has been constructed to show the length of flaw needed to cause sub-critical crack propagation before and after rain (using $H_s = 0.12$ m and $\Delta\tau_g = 10$ Pa to simulate conditions 15 minutes after rain starts). The separate effects of the additional loading and alterations to the slab modulus are shown. The plot is truncated at small values of τ_p/τ_g (before rain), because the extra loading from rain increases sufficiently so that $\tau_g = \tau_p$ and immediate failure is expected. For cases where the stability index is higher, rain-induced alterations reduce the length of flaw needed to initiate sub-critical crack growth by 10–20%. Such changes (~2 m or less) are small but the abrupt increase in avalanche activity soon after the onset of rain implies the changes are sufficient to initiate sub-critical crack propagation and ultimately rapid dynamic failure.

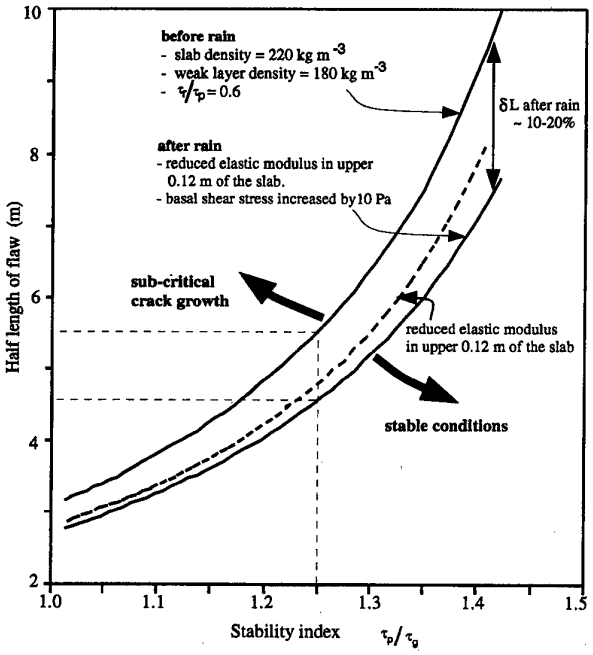

Fig. 4. Half-length of flaw needed to cause sub-critical crack growth as a function of the stability index τ_p/τ_g before and after rain. The intermediate dashed curve shows the impact when only the elastic modulus in the upper 0.12 m of the slab is reduced. The envelope between the solid curves gives the range of possible basal conditions before rain. For example (for $\tau_p/\tau_g = 1.25$), a flaw of half-length smaller than 5.6 m could have existed without expanding before rain but it must have been larger than 4.6 m for the slope to fail immediately after rain started.

The analysis supports observations that freshly deposited snow is often unstable. For example, for conditions given in Figure 4 and $\tau_p/\tau_g = 1.25$, the model predicts that before rain the slope must have contained a flaw of half-length between 4.6 and 5.6 m, because rain-induced alterations would not be sufficient to initiate sub-critical crack propagation from a smaller flaw, and propagation would have begun before rain started if the flaw were larger. This rather narrow band of pre-failure conditions is more likely to exist in freshly deposited snow, because sintering processes usually act to increase the strength of snow with time. Our observations indicate that abrupt and widespread avalanche activity is rare when rain falls on older, well-bonded snowpacks.

Model results may also yield insight into skier-released avalanches. A ski-cut about 0.1 m deep would reduce the "effective" slab thickness at least locally and have a similar impact to that shown in Figure 4 (even without accounting for all the additional stress imposed by the skier). Observations indicate that rain is a more effective trigger of new snow avalanches than ski-cutting (personal communication from C. Wilbour, 1996). The difference may be that rain-induced alterations occur over a wide region and perturb all existing imperfections in the snowpack. A skier might miss cutting across a flawed zone.

CONCLUSIONS

Measurements of snow properties and stratigraphic observations at slab-avalanche fracture lines provide the basis for adapting a slip-weakening model in which slip at the bed is non-uniform and the basal shear strength degrades to a residual strength with ongoing slip. Non-uniform slip implies the existence of crack-like flaws or imperfections in the basal layer, where stresses from the overburden are not fully supported. As the flaw-size increases, stress concentrations at the edges will cause sub-critical crack growth and subsequent rapid-failure propagation. Using values typical for properties measured at avalanche fracture-line profiles, the model predicts sub-critical crack growth can initiate from a relatively small flaw, well before the gravitational shear stress approaches the peak basal shear strength. This result is consistent with field observations and measurements at avalanche-fracture lines.

Measurements indicate that alterations induced by rain on new snow are usually restricted to the upper 0.15 m of the snowpack. The slip-weakening model predicts such surface alterations will reduce the length of flaw needed to initiate sub-critical crack growth by just 15–20%. Apparently, this relatively small perturbation is sufficient to cause the abrupt change in stability often observed at the onset of rain. Conditions prior to rain must have been close to critical, which is consistent with field observations that indicate freshly deposited snow is often very unstable.

The slip-weakening model shows that the slab modulus can have a controlling influence on slope stability; it is evident that both the slab and the weak layer act together to control slope stability. Most field practioners focus on the basal layer, when searching for a stability index, but it may also be useful to examine the properties of the slab for clues about snow-slope stability.

ACKNOWLEDGEMENTS

This research was funded by the U.S. Army Research Office (grant No. DAAH04-95-1-0172) and their support is gratefully acknowledged. I also wish to thank R. Benedict, S. Breyfogle, R. Gibson, H. -P. Marshall, L. A. Rasmussen, L. Reddon and C. Wilbour for assistance. Comments by J. Johnson, D. McClung and C. F. Raymond greatly improved an earlier version of this manuscript.

REFERENCES

Conway, H. and J. Abrahamson. 1984. Snow stability index. *J. Glaciol.*, **30**(106), 321–327.

Conway, H. and R. Benedict. 1994. Infiltration of water into snow. *Water Resour. Res.*, **30**(3), 641–649.

Conway, H. and C. F. Raymond. 1993. Snow stability during rain. *J. Glaciol.*, **39**(133), 635–642.

De Montmollin, V. 1982. Shear tests on snow explained by fast metamorphism. *J. Glaciol.*, **28**(98), 187–198.

Gibson, L. J. and M. F. Ashby. 1987. *Cellular solids: structure and properties.* New York, Pergamon Press.

Jamieson, J. B. 1995. Avalanche prediction for persistent snow slabs. (Ph.D. thesis, University of Calgary.)

Kry, P. R. 1975. Quantitative stereological analysis of grain bonds in snow. *J. Glaciol.*, **14**(72), 467–477.

Li, V. C. 1987. Mechanics of shear ruptures applied to earthquake zones. *In* Atkinson, B.K., *ed. Fracture mechanics of rocks.* San Diego, CA, Academic Press, 351–428.

McClung, D. M. 1977. Direct simple shear tests on snow and their relation to slab avalanche formation. *J. Glaciol.*, **19**(81), 101–109.

McClung, D. M. 1979. Shear fracture precipitated by strain softening as a mechanism of dry slab avalanche release. *J. Geophys. Res.*, **84**(B7), 3519–3526.

McClung, D. M. 1981. Fracture mechanical model of dry slab avalanche release. *J. Geophys. Res.*, **86**(B11), 10,783–10,790.

McClung, D. M. 1996. Effects of temperature on fracture in dry slab avalanche release. *J. Geophys. Res.*, **101**(B10), 21,907–21,920.

McClung, D. M. and P. A. Schaerer. 1993. *The avalanche handbook.* Seattle, WA, The Mountaineers.

Mellor, M. 1975. A review of basic snow mechanics. *International Association of Hydrological Sciences Publication* 114 (Symposium at Grindelwald 1974 — *Snow Mechanics*), 251–291.

Palmer, A. C. and J. R. Rice. 1973. The growth of slip surfaces in the progressive failure of over-consolidated clay. *Proc. R. Soc. London, Ser. A*, **332**(1591), 527–548.

Perla, R., T. M. H. Beck and T. T. Cheng. 1982. The shear strength index of alpine snow. *Cold Reg. Sci. Technol.*, **6**(1), 11–20.

SNOW DENSIFICATION DURING RAIN

H.P. Marshall[1], H. Conway and L.A. Rasmussen

Geophysics Program, University of Washington, Seattle, WA 98195, U.S.A.

Abstract: Observations and measurements indicate rain often has a major impact on snow slope stability. Measurements to investigate the effects of wetting of low density, alpine snow were made at Snoqualmie Pass, Washington, U.S.A. Results indicate that on first wetting the densification rate can increase by three orders of magnitude. This initial burst of densification occurs independently of the gravitational load and is probably a result of rapid structural changes and grain rearrangement that occurs when liquid water is first introduced. The rate decreases rapidly with time, although it remains about two orders of magnitude higher than that for dry snow of the same density. The rate of densification decreases as density increases. We assume snow behaves as a linear viscous fluid and that the metamorphic and gravitational components of compaction are additive. A simple model of compaction is derived empirically using the measurements. The model fits the measurements very well, although more experiments are needed to determine the dependence of the model parameters on liquid water content.

Keywords

Snow, snow compaction, rain on snow

1. Introduction

Widespread avalanche activity is often observed immediately following the onset of rain. Previous work has shown that the avalanching occurs both before the rain has reached the sliding layer, and before the increase in overburden stress due to the additional weight of water would have caused the slope to fail [*Conway and Raymond*, 1993]. The failure layer is dry at the time of avalanching, and apparently surface perturbations caused by the rain are sufficient to alter slope stability. Here we present and discuss measurements of compaction of natural snowpacks during rain and also experiments in which water was introduced artificially.

Compaction of dry snow at low strain rates has been the subject of numerous studies, many of which have been discussed in reviews such as [*Bader*, 1962], [*Mellor*, 1975], [*Salm*, 1982], [*Shapiro et al.*, 1997]. Accurate descriptions of micro-structural properties are needed to formulate a realistic physical model of snow densification [e.g., *Keeler*, 1969; *Hansen and Brown*, 1987] but application of this type of model is difficult because micro-structural properties are not easily measured. Empirical models are easier to apply and often provide a better fit to measurements than do physical models [*Colbeck et al.*, 1978; *Herron and Langway*, 1980], although caution is needed when applying these models outside the range of the experimental data used to formulate them. Empirical models continue to be used in practical applications [e.g., *Schweizer*, 1993; *Bader and Salm*, 1990] and it is likely that they will remain in use until an easily measured micro-structural parameter is identified.

The vertical rate of compaction $\dot{\varepsilon}_{zz}$ (for positive z in the downward direction), or densification rate $\frac{1}{\rho(t)}\frac{d\rho}{dt}$, of natural snow in response to stress from the overburden $\sigma_{zz}(t) = \int \rho(t) g dz$ is often described by a one dimensional constitutive relationship for a linear viscous fluid [e.g., *Kojima*, 1967]. Metamorphic processes also cause snow density to change independently of gravity and it is convenient to think of the metamorphic component $\sigma_m(t)$ as a stress that is additive to the gravitational stress:

$$\dot{\varepsilon}_{zz} = \frac{1}{\rho(t)}\frac{d\rho}{dt} = \frac{1}{\eta_{zz}}(\sigma_m(t) + \sigma_{zz}(t)) \qquad (1)$$

Experiments show the compactive viscosity $\eta_{zz}(t)$ varies exponentially with density [*Kojima*, 1967], temperature T and liquid water content w of the snow [*Yamazaki et al.*, 1993] and can be written:

$$\eta_{zz}(t) = A_1(w)\, A_2\, e^{A_3 \frac{\rho(t)}{\rho_i}}\, e^{E/RT} \qquad (2)$$

where $A_1(w)$ decreases exponentially from 1.0 for dry snow to 10^{-5} at 14% water content [*Yamazaki et al.*, 1993], $A_2 = 1.1 \times 10^{-8} Pa \cdot min$, $A_3 = 19.3$, the density of ice $\rho_i = 917\, kg\, m^{-3}$, the activation energy $E = 67.3\, kJ\, mol^{-1}$, and the gas constant $R = 0.00831\, kJ\, mol^{-1}\, K^{-1}$.

[1]Corresponding author address: H.P. Marshall, Geophysics Program, Box 351650, University of Washington, Seattle, WA 98195-1650; tel: 206-616-5393; email: hpm@geophys.washington.edu

2. Observations and measurements during rain on snow

We have made high resolution measurements of compaction of natural snow at the Washington State Department of Transportation snow study site (915 m a.s.l.) at Snoqualmie Pass, Washington U.S.A. Mid-winter storms often deposit up to 1 m of new snow which may then be followed by rain. Widespread avalanching is often observed immediately following the onset of rain [*Conway and Raymond*, 1993].

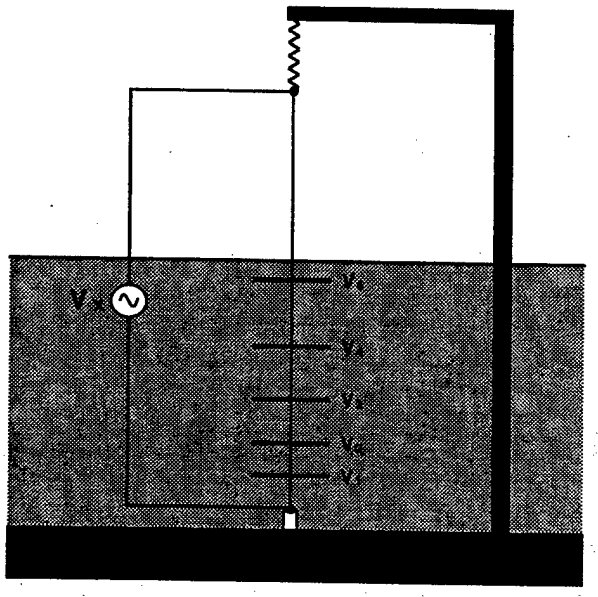

Figure 1. Apparatus for measuring settlement within snowpacks.

Fig. 1 shows the apparatus used to measure settlement within snowpacks. Velocity shoes made from light-weight aluminum screening were placed sequentially at the surface after 10 to 30 cm of incremental snow accumulation. A sliding contact mounted on each shoe made electrical contact with a resistance wire strung between a support above the surface and the ground. We configured this as a voltage divider circuit to calculate the shoe position with an accuracy of $\pm 2\,mm$. Thermistors attached to the shoes measured the temperature in the snow at each shoe position. Measurements, usually made at 15 minute intervals, were recorded using a datalogger and storage module. The evolution of layer density was calculated from measurements of the initial snow density and changes in layer thickness.

Other things being equal, the increased stress from the overburden should cause layers at depth to densify more rapidly than layers near the surface (Eqn. 1). However in reality the snow at depth is likely to be more dense (and hence more viscous - Eqn. 2), and/or during rain, the surface layers will be wetted first (because of the time lag of infiltration). Both effects complicate interpretation of measurements of settlement in natural conditions.

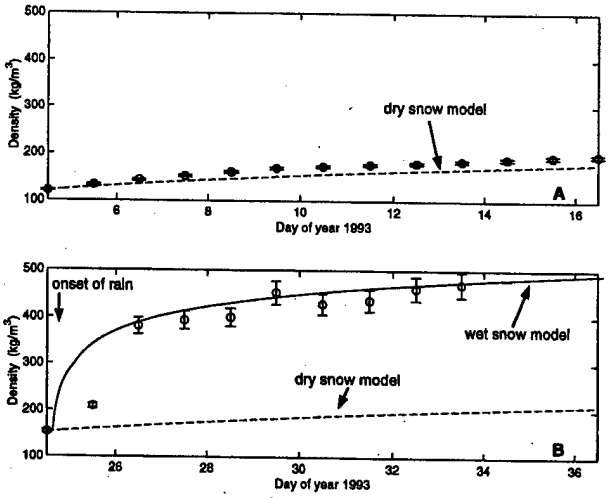

Figure 2. Densification of two layers of natural snow using the apparatus shown in Fig. 1. Fig. 2A shows a layer which was dry throughout the measurement period, while figure 2B shows a layer which became wet after rain started. The error bars for Fig. 2A are within the symbols. For comparison, in both cases the dashed lines show results from the dry snow model (Eqn. 1). The solid line (Fig. 2B) shows results from the wet snow model (Eqns. 4 and 5).

Fig. 2 shows measured compaction rates in natural snow for two layers in 1993. Both layers were near the surface during measurements; Fig. 2A shows a layer which was dry throughout the measurement period ($-5.4 < T_{snow} < -3.5°C$). Fig. 2B shows a layer that was wetted by rain which started at 1500 hr on day 24. The uncertainty in the estimate of density was calculated using propagation of errors [*Bevington and Robinson*, 1992], assuming the error in velocity shoe position was $\pm 2mm$, the error in the measurement of water equivalent was $\pm 0.25\,mm$, and that the two errors were uncorrelated. For comparison, model predictions for dry snow (Eqn. 1) are also shown. We expect values of $\sigma_m(t)$ will range from being positive (equilibrium metamorphism) to negative under large temperature gradients (kinetic growth metamorphism). Here for dry snow we use a constant value evaluated by fitting measurements of density of dry snow near the surface ($\sigma_{zz} \approx 0$) to Eqn. 1. Results from four such experiments yielded an average $\sigma_m(t) = 75 \pm 35\,Pa$ which is equivalent to about 7.5 mm (water equivalent) overburden. The solid line (Fig. 2B) shows

results from the wet snow model discussed later.

Results show the dry-snow layer (Fig. 2A) densified slightly faster than the model prediction (assuming $\sigma_{zz} = 0$). However the difference is well within the model uncertainty (uncertainties in $\rho(0)$, $\sigma_m(t)$ and temperature) and further, some snow accumulated during the experiment making $\sigma_{zz} > 0$. In contrast, the wet layer densified more than 100× faster than the model prediction for dry snow (Fig. 2B). Introduction of liquid water has a major impact on the rate of densification and below we discuss experiments to investigate this effect.

3. Experiments to investigate the first wetting of dry snow

Experiments were done during the 1996-97 winter at Snoqualmie Pass. Undisturbed samples of freshly deposited snow were collected by pressing a cylindrical container into the new snow, sliding a sheet of plywood underneath and then inverting it. The average initial density $\rho(0)$ was obtained by subtracting the weight of the empty container from the weight when filled with snow, and dividing by the sample volume. A known volume of water at 0°C was sprayed evenly over the surface. Changes in height of snow in the container were measured as a function of time for up to five hours and used to calculate changes in density. The change in height at a given time was taken to be the average of five measurements across the center of the sample (Fig. 3). A large can ($h = 160\,mm$, $diam. = 155\,mm$) was used for four of the experiments, and plastic containers ($h = 70\,mm$, $diam. = 167\,mm$) were used for the others. In each experiment about 14% (by volume) of water was distributed evenly over the surface within ~ 30 seconds.

The experiments were done outdoors and were therefore subject to changing environmental conditions. When the air temperature was lower than ~ −5°C the water froze at the surface and infiltration was impeded. At temperatures higher than ~ +1°C the snow melted, and measured changes in height were the combined effects of loss of ice mass and densification. To reduce melting during warm conditions we buried the container (with the top level with the surface) within the natural snow. A total of 20 experiments were successfully completed within the range $-5^o < T_{air} < 1^oC$.

We are not certain how the container size affects the measurements. In most experiments the change in volume was caused by changes in height with little shrinkage from the sides and we suspect that edge effects were minor. However it would be useful to do more experiments with containers of varying diameter to determine when edge effects become important.

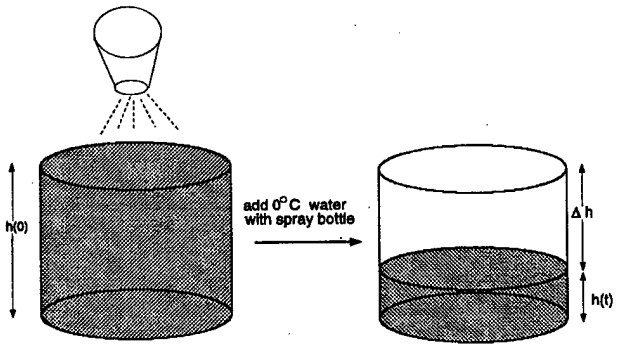

Figure 3. Densification experiments. Water was sprayed uniformly onto a volume of snow with initial height $h(0)$ and density $\rho(0)$. The height at time t after first wetting $h(t)$ was calculated by measuring $\Delta h(t)$ at 1 minute intervals for the first 10 minutes, and every 10-30 minutes thereafter for up to 5 hours. $\Delta h(t)$ was the average of 5 measurements across the center of the sample.

The standard deviation of each measurement of density $S_{\rho(t)}$ was calculated from the uncertainty in the measurement of mass ($S_M = \pm 1g$), radius of the sample cylinder ($S_r = 0.5mm$) and height ($S_h^2 = S_{hp}^2 + S_{ha}^2$ where the accuracy of height measurement $S_{ha} = 0.5mm$ and the precision of height measurement S_{hp} is the standard deviation of the five measurements). Assuming the errors are uncorrelated, the uncertainty in density is [*Bevington and Robinson*, 1992]:

$$(\frac{S_{\rho(t)}}{\rho(t)})^2 = (\frac{S_h}{h(t)})^2 + (\frac{S_M}{M})^2 + (\frac{2S_r}{r})^2 \qquad (3)$$

where M= the total mass of the sample, r is its radius, and $h(t)$ is its height. Because the surface becomes more irregular with time, and h(t) decreases, the standard deviation increases with time.

Fig. 4 shows results from two experiments. One ($\rho(0) = 125\,kg\,m^{-3}$) is typical of fourteen experiments in which the initial density ranged from 100 to 190 $kg\,m^{-3}$. Low-density snow always densified rapidly in the first few minutes after wetting, and the rate decreased as densification proceeded. On the other hand, changes were too small to be detected over the period of measurements when the initial density was high such as in the other experiment ($\rho(0) = 360\,kg\,m^{-3}$). The rate of densification for snow of low initial density was much faster than that predicted by the dry snow model. This is not surprising since we expect rapid structural changes and grain rearrangement when liquid water is first

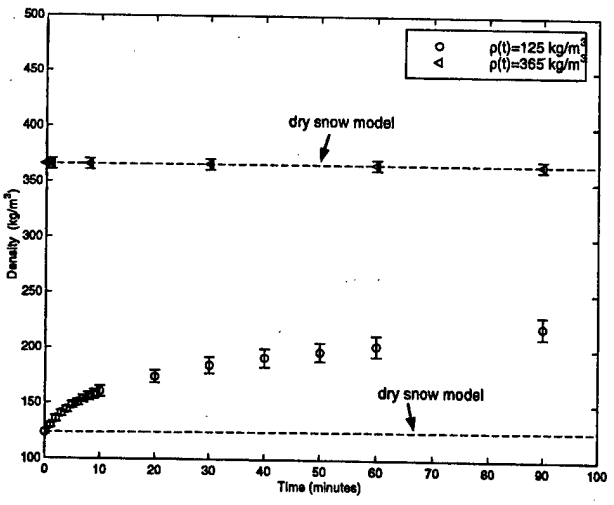

Figure 4. Evolution of snow density $\rho(t)$ calculated from measurements of $\rho(0)$ and $h(t)$ for $\rho(0) = 120 kg\,m^{-3}$, and $\rho(0) = 360 kg\,m^{-3}$. In both cases 14% (by volume) of water was added at $t = 0$. The densities plotted are *dry* density - that is without the liquid water. The dashed lines show the dry snow model for comparison.

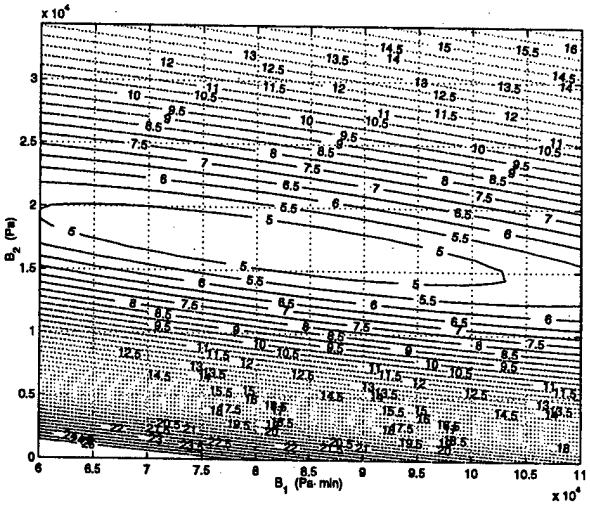

Figure 5. Optimization of model parameters B_1 and B_2. The optimum values ($B_1 = 8.0 \times 10^4 Pa\,min$, $B_2 = 1.65 \times 10^4 Pa$) gave $\overline{S} < 4.6\ kgm^{-3}$.

introduced to low density snow, and at higher densities we expect the presence of liquid water would lubricate grain boundaries and enhance densification [*Colbeck et al.*, 1978].

3.1 Model development

We use a similar formulation to that used for dry snow (Eqns. 1 and 2) but with different values for the model parameters. For a first approximation we assume $\eta_{zz(wet)} = A_1 \times \eta_{zz(dry)}$. $T = 273°K$ for wet snow and σ_{zz} is small (ranging from 0 at the surface to $\sim 140\,Pa$ at the bottom of the container) compared with other effects during wet snow compaction and here we ignore it. For the experimental conditions we rewrite Eqn.1:

$$\frac{1}{\rho(t)}\frac{d\rho}{dt} = \frac{1}{A_1\,\eta_{zz(dry)}}(\sigma_m(t) + 0) \qquad (4)$$

Eqn.4 is not easily integrated and instead we solve for $\rho_z(t)$ iteratively using 1 minute time steps. A constant value for $\sigma_m(t)/A_1$ does not capture the rapid densification when water is first added to dry snow and we use a time dependent function:

$$\frac{\sigma_m(t)}{A_1} = \frac{B_1}{t} + B_2 \qquad (5)$$

The term B_1/t captures the rapid initial change. $B_1/t \to 0$ as $t \to \infty$, and so B_2 models the long term impact of wetting.

The root mean square error S_k for each experiment is calculated from:

$$S_k = \sqrt{\frac{1}{N_k}\sum[\rho_k(t) - \rho^*(t)]^2} \qquad (6)$$

where $\rho_k(t)$ is the measured density at time t, $\rho^*(t)$ is the modeled density (from Eqn. 4), and N_k is the number of measurements.

We choose B_1 and B_2 to minimize the average root mean square error $\overline{S}$ for all 20 experiments:

$$\overline{S} = \sqrt{\frac{1}{20}\sum(S_k)^2} \qquad (7)$$

Fig. 5 shows results of the optimization which indicate (for t in minutes) $B_1 = 8.0 \times 10^4\,Pa\,min$, $B_2 = 1.65 \times 10^4\,Pa$. The average rms ($4.59\ kgm^{-3}$) is small considering that the density of a natural snow layer can vary by up to 10%. Fig. 6 shows measured and modeled results for five experiments. For most experiments, the model was within the measurement error. In the few places where the model did not match the measurements it is possible that densification was affected by a change in conditions. For example in the experiment shown with $\rho(0) = 100\,kgm^{-3}$ the rate of densification slowed between 50 and 125 minutes, probably because the air temperature decreased during that time.

4. Discussion

The model developed for wet snow densification from the experiments fits the measurements made in the natural snowpack during rain on January 24,

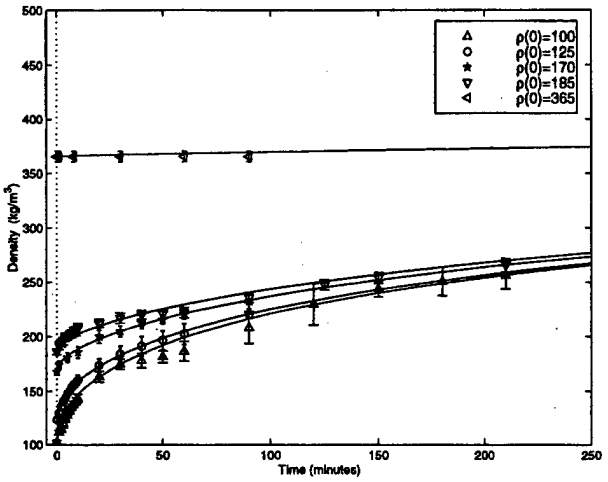

Figure 6. Measurements and model results during first wetting of low density snow. The plot shows five experiments with snow of different initial densities. The rate of densification increased with introduction of liquid water, and decreased as the density increased. The increase was especially fast during the first 10 minutes.

1993 (solid line in Fig. 2B) remarkably well. Precipitation rates at Snoqualmie Pass are typically $\sim 10\,mm\,hr^{-1}$. Observations indicate liquid water is usually contained within the upper 7–10 cm of the snowpack during the first hour, which implies a water content of 10 to 15% (by volume) after one hour. In our experiments the snow samples reached a similar water content much more quickly, and this difference in application rate is most likely the reason the measurement immediately after the onset of rain deviates slightly from the model (Fig. 2B).

We expect both the viscosity and the metamorphic components will change when liquid water is introduced to dry snow. We are unable to resolve the separate contributions from our data (Eqn. 5) but we can compare the increase in compaction rate during wetting (no load conditions) from the ratio $\dot{\epsilon}_{zz(wet)} : \dot{\epsilon}_{zz(dry)}$ which reduces to $\frac{1}{75}(B_1/t + B_2)$. Hence the addition of water increases the compaction rate more than 1000× in the first minute, and even as $t \to \infty$ (> 100 minutes) the rate is still $\sim 200\times$ faster than for dry snow. We note that in our experiments the amount of liquid water ($\sim 14\%$ by volume) was not varied. We suspect the model parameters depend strongly on both the water content [*Yamazaki et al.*, 1993] and the application rate. It would be useful to do more experiments to determine the dependence of the model parameters on both the rate of application and the liquid water content.

We note that our results suggest the rate of densification in wet snow is much faster than that commonly used in the literature [e.g. *Anderson*, 1976; *Jordan*, 1991]. Even the long-term rate is about two orders of magnitude faster than the more commonly used value. It is possible that the difference arises because the liquid water content in a natural snowpack consisting of well rounded grains is likely to be somewhat less than 14% and the viscosity is strongly dependent on water content [*Yamazaki et al.*, 1993].

It is dangerous to extrapolate (because the model was formulated using measurements over less than a day) but the model predicts the snow density will be $550\,kg\,m^{-3}$ (the density of equal-sized, close-packed spheres of ice) after about 35 days and about $600\,kg\,m^{-3}$ after 90 days. We are not certain whether our model is applicable over this time scale but it is interesting to note that end of season measurements at Blue Glacier in the Olympic mountains (typically after about 90 days of melt) indicate the residual snow density is similar ($\sim 580\,kg\,m^{-3}$).

It is likely that the burst in densification at the onset of rain is a result of grain rearrangement and structural changes. It has been suggested that this rapid alteration in mechanical properties at the surface has a controlling influence on snow slope stability at the onset of rain [*Conway*, 1998]. It would be useful to investigate this further, and in particular, measure the evolution of the vertical distribution of liquid water together with densification rates through natural snowpacks after the onset of rain.

5. Conclusions

The simple model for compaction of wet snow fits our measurements very well but more experiments are needed to determine the dependence of model parameters on liquid water content. The model captures the essential features observed on first wetting of dry snow. These are:

- on first wetting the densification rate increases by three orders of magnitude. We suspect this initial burst of densification is caused by rapid structural changes and grain rearrangement when liquid water is first introduced.
- the rate decreases rapidly with time although it remains about two orders of magnitude higher than for dry snow of the same density. We suspect the presence of liquid water reduces friction at grain boundaries which would increase the rate of densification.
- as with dry snow, the rate of densification decreases as density increases.

References

Anderson, E. A., A Point Energy and Mass Balance Model of a Snow Cover, NOAA Technical Report NWS No. 19, 1976.

Bader, H., The physics and mechanics of snow as a material, CRREL Technical Monograph II-B, 79pp, 1962.

Bader, H.-P., and B. Salm, On the mechanics of snow slab release, *Cold Regions Science and Technology*, *17*, 287–300, 1990.

Bevington, P. R., and D. K. Robinson, *Data Reduction and Error Analysis for the Physical Sciences, 328pp.*, McGraw-Hill, 2nd ed., New York, 1992.

Colbeck, S. C., K. A. Shaw, and G. Lemieux, The compression of wet snow, CRREL Technical Report 78-10, 23pp., 1978.

Conway, H., The impact of surface perturbations on snow-slope stability, *Ann. Glaciol.*, *26*, 307–312, 1998.

Conway, H., and C. F. Raymond, Snow stability during rain, *J. Glaciol.*, *39*(133), 635–642, 1993.

Hansen, A. C., and R. L. Brown, A new constitutive theory for snow based on a micro-mechanical approach, in *Avalanche Movement and Effects. Proc. Davos Symposium*, no. 162, pp. 87–104, Int. Ass. Hydrol. Sci., 1987.

Herron, M. M., and C. C. Langway, Firn densification: An empirical model, *J. Glaciol.*, *25*(93), 373–385, 1980.

Jordan, R., A one-dimensional temperature model for a snow cover, CRREL Special Report 91-16, 49pp., 1991.

Keeler, C. M., The growth of bonds and the increase of mechanical strength in a dry seasonal snow-pack, *J. Glaciol.*, *8*(54), 441–450, 1969.

Kojima, K., Densification of seasonal snowcover, in *Physics of Snow and Ice, Proc. Int. Conf. on Low Temp. Sci.*, edited by H. Oura, vol. 1, pp. 929–952, Hokkaido Univ., Sapporo, 1967.

Mellor, M., A review of basic snow mechanics, *Int. Ass. Hydrol. Sci.*, *114*, 251–291, 1975.

Salm, B., Mechanical properties of snow, *Reviews of Geophysics and Space Physics*, *20*(1), 1–19, 1982.

Schweizer, J., The influence of the layered character of snow cover on the triggering of slab avalanches, *Ann. Glaciol.*, *18*, 193–198, 1993.

Shapiro, L. H., J. B. Johnson, M. Sturm, and G. L. Blaisdell, Snow mechanics: Review of the state of knowledge and applications, CRREL Technical Report 97-3, 36pp., 1997.

Yamazaki, T., J. Kondo, T. Sakuraoka, and T. Nakamura, A one-dimensional model of the evolution of snow-cover characteristics, *Ann. Glaciol.*, *18*, 22–26, 1993.

Corresponding author address: H. P. Marshall, Geophysics Program, University of Washington, Box 351650, Seattle, WA 98195-1650; tel: 206-616-5393; email: hpm@geophys.washington.edu

This preprint was prepared with AGU's LaTeX macros v4, with the extension package 'AGU++' by P. W. Daly, version 1.5d from 1997/04/28.

Acknowledgments

This research was funded by the U.S. Army Research Office (Grant No. DAAH04-95-1-0172). We also thank the Washington State Department of Transportation for logistical support and Don Marshall for help with model development.

EVOLUTION OF SNOW SLOPE STABILITY DURING STORMS

H. Conway and C. Wilbour

Geophysics Program, University of Washington and Washington State Department of Transportation, Snoqualmie Pass

Abstract: The evolution of snow slope stability during storms is investigated using simple models to calculate the shear strength of a buried layer (from its density) and the imposed shear stress (from the weight of the overburden). There is a competition between the rate of loading from new snowfall and the rate of strengthening of buried layers. In theory, unstable conditions will occur when the stability index $\Sigma_z(t)$ (the ratio of the shear strength of a buried weak layer at depth z to the shear stress imposed by the overburden) approaches 1.0. A related index of practical interest is the expected time to failure (the time when $\Sigma_z(t)$ will become critical if the current conditions continue). The model is tested using measurements and observations of avalanche activity during three storm cycles at Snoqualmie Pass in the Washington Cascades. In two cases the avalanche activity was high while in the other, few avalanches released. $T_f(t)$ proved to be a better discriminator between stable and unstable conditions than $\Sigma_z(t)$. This is because it contains information about both the *magnitude* and the expected *changes* of $\Sigma_z(t)$ in response to the current conditions. Even if $\Sigma_z(t)$ is close to critical, if it is not decreasing then slopes will remain stable. Results indicate the model may prove useful for forecasting avalanches during storms. The required input (hourly measurements of precipitation, air temperature and new snow density) is routinely measured at many study sites and the tractability of the model makes it attractive for operational use.

Keywords

Storm and avalanche cycles, snow slope stability.

Introduction

Observations indicate that most natural dry snow slab avalanches release as a result of rapid loading from snowfall [*McClung and Schaerer*, 1993]. Here we examine the evolution of snow slope stability during storms. Of particular interest is to determine the conditions that cause these direct-action avalanches.

Models of dry snow slope failure show two conditions must be satisfied before slab avalanches will release: (i) the downslope component of the weight of the slab must be close to the average shear strength of a buried weak layer; (ii) the rate of deformation within the buried weak layer must be sufficiently high to cause failure [*McClung*, 1981; *Gubler and Bader*, 1989; *Bader and Salm*, 1990]. The probability of failure increases when the stability index Σ_z (the ratio of the shear strength of a buried weak layer at depth z to the shear stress imposed by the overburden) approaches 1.0 [*Perla and LaChapelle*, 1970].

In contrast, shear frame measurements at fracture lines on failed slopes typically yield average values of $\overline{\Sigma}_z$ greater than 1.0 [*Roch*, 1966; *Sommerfeld and King*, 1979; *Jamieson*, 1995]. In addition, measurements show high variability which led *Perla* [1977] to doubt the usefulness of such measurements. However an index of stability has continued to be popular among field practitoners and tests such as the Rutschblock [e.g., *Fohn*, 1987; *Jamieson and Johnson*, 1993a] or the shovel shear test [e.g., *Schaerer*, 1989; *Jamieson and Johnson*, 1993b] are designed to examine the relationship between strength of the weak layer and the stress from the overburden.

There is a strong motivation to improve predictions of snow slope stability. Here we do not attempt a rigorous analysis of the coupled thermal-mechanical conditions expected in snow slabs, but rather we investigate the evolution of the strength of buried weak layers and the applied static stress from the overburden during storms. Our goal is to find an *index* that can be used as a tool in operational avalanche forecasting.

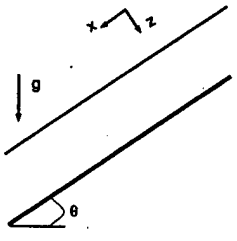

Figure 1. Coordinate convention used for planar snow slab inclined at angle θ.

Evolution of the stability index

Basal shear stress

Neglecting longitudinal stresses, the average static shear stress $\sigma_{xz}(t)$ at depth z and time t in a planar slab inclined at angle θ (Fig.1) during times of precipitation is:

$$\sigma_{xz}(t) = g \int P_w cos\theta sin\theta \, dt \qquad (1)$$

where the gravitational constant $g = 9.8\, m\, s^{-2}$ and P_w is the rate of accumulation (measured in the earth vertical direction). In theory, gauge measurements of precipitation from a representative site could be used in Eqn.1, but in practice, interactions between winds and complex topography make it difficult to accurately predict the spatial and temporal pattern of accumulation.

Basal shear strength

Estimating the shear strength of a buried weak layer is also problematic. The mechanical properties of snow depend strongly on microstructure [*Keeler*, 1969; *Hansen and Brown*, 1987] but the relevant microstructural properties are generally not known nor measured. Although not ideal, bulk density is more easily (and more often) measured and mechanical properties undergo significant improvement with densification. We follow an approach used by *Gibson and Ashby* [1987] who modeled cellular solids as rods of length l and thickness d. For this geometry, snow density ρ_s is approximately:

$$\rho_s = A_1 \rho_i (\frac{d}{l})^2 \qquad (2)$$

where ρ_i, the density of ice is $917\, kg\, m^{-3}$, and A_1 is a shape factor that depends on the grain structure. Further analysis makes use of beam theory, and assuming failure after a critical displacement (elastic behavior), the shear fracture strength σ_f is:

$$\sigma_f = A_2 (\frac{\rho_s}{\rho_i})^2 \qquad (3)$$

The model parameter A_2 includes the Youngs's modulus of ice as well as A_1. Although this model is deficient, experiments show such a power law relationship explains much of the variability in measurements [*Perla et al.*, 1982; *Jamieson*, 1995]. Fig.2 shows Jamieson's measurements which indicate A_2 varies from about 1.8×10^4 Pa for open grain structures (such as faceted grains) to 2.2×10^4 Pa for partly metamorphosed new snow. We expect values to be log-normally distributed (the strength can

not be negative) and the best fit to all measurements ($A_2 = 1.95 \times 10^4$ Pa) has $r^2 = 0.66$ and $rms = 0.61\,\sigma_f\,Pa$. Structural differences that cause variations in strength of snow of the same density are not accounted for in this simple model and probably cause much of the uncertainty. Errors associated with measurements of density (particularly in thin layers where accurate measurements are difficult to obtain) may also contribute.

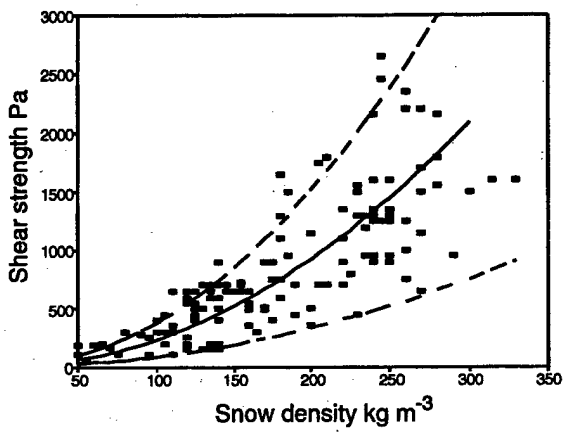

Figure 2. Measurements of shear strength σ_f and snow density ρ_s by *Jamieson* [1995]. The solid line is the best fitting power law relationship ($r^2 = 0.66, rms = 0.61\sigma_f Pa$) and the dashed lines are ± the standard deviation.

Both metamorphic processes and the stress from the overburden $\sigma_{zz}(t)$ contribute to cause the density of a dry snow layer to change during a storm cycle. It is convenient to think of the metamorphic component as a stress $\sigma_m(t)$ that simply adds to the gravitational stress and assume a viscous densification law for dry snow of density $\rho_z(t)$ at depth z of the form:

$$\frac{1}{\rho_z(t)}\frac{d\rho_z}{dt} = \frac{1}{\eta_{zz}(t)}[\sigma_m(t) + \sigma_{zz}(t)] \qquad (4)$$

Eqn.4 applies to a horizontal snowpack but here we neglect the effect of shear on densification and apply the same expression for inclined snowpacks using $\sigma_{zz}(t) = g \int P_w cos^2\theta\, dt$. This assumption is not too restrictive because the Poisson ratio $\nu \to 0$ for low density snow. The kinetic term $\eta_{zz}(t)$ is the compactive viscosity often used to represent a viscous constitutive relationship for dry snow [e.g., *Kojima*, 1967] modified with an Arrhenius type temperature term:

$$\eta_{zz}(t) = B_1 e^{B_2(\frac{\rho_z(t)}{\rho_i})} e^{E/(RT_z)} \qquad (5)$$

When $B_1 = 6.5 \times 10^{-7}\,Pa\,s, B_2 = 19.3$, the activation energy $E = 67.3\,kJ\,mol^{-1}$, the gas constant $R = 0.0083\,kJ\,mol^{-1}\,{}^oK^{-1}$, the layer temperature T_z is in ${}^oK$, then η_{zz} is in units of Pa s.

We expect values of $\sigma_m(t)$ will range from being positive (equilibrium metamorphism) to negative under large temperature gradients (kinetic growth metamorphism). During storms we expect conditions are more conducive for equilibrium metamorphism and use a constant value ($75\,Pa$) which is the average found from compaction measurements near the surface where $\sigma_{zz}(t) \approx 0$ [*Marshall et al.*, submitted]. Using $\sigma_m = 75\,Pa$ implies that densification is dominated by metamorphic processes near the surface, but the gravitational component controls in layers more than 5 to 10 cm below the surface.

Stability index and time to failure

The average stability index $\overline{\Sigma}_z(t)$ at depth z and time t is:

$$\overline{\Sigma}_z(t) = \frac{\sigma_{fz}(t)}{\sigma_{xz}(t)} \qquad (6)$$

$\sigma_{xz}(t)$ comes from Eqn.1 and we solve for $\rho_z(t)$ iteratively (Eqns.4 and 5) and use these in Eqn.3 to calculate $\sigma_{fz}(t)$.

Of special interest for operational purposes is the expected time to failure $T_f(t)$ which is:

$$T_f(t) = \frac{(\overline{\Sigma}_z(t) - 1.0)}{d\overline{\Sigma}_z/dt} \qquad (7)$$

$T_f(t)$ contains information about how the current conditions are affecting $\Sigma_z(t)$ and when it will reach its critical value.

Model uncertainties

There are two contributions to the uncertainty in strength. The first comes from the inexactness of the strength-density relationship ($0.61\,\sigma_f$ - see Fig.2) and the other comes from the uncertainty in density. We assume the measurements of density have an error ±10% so its contribution to the uncertainty in strength (a power law function of density) is $2 \times 0.1\,\sigma_f$. If the two components are not correlated the total uncertainty is $\sqrt{(0.61)^2 + (0.2)^2} \times \sigma_f$ or $0.64\,\sigma_f$ [*Bevington and Robinson*, 1992]. If measurements of precipitation are also subject to ±10% error, the uncertainty in shear stress is ±10%. The total uncertainty in the stability index is $\sqrt{(0.64)^2 + (0.1)^2} \times \Sigma_z$ or $0.65\,\Sigma_z$ [*Bevington and Robinson*, 1992].

Sensitivity studies

The rate of densification (and hence strengthening) of a buried layer increases with load from the overburden (Eqn.4). Although the snow is weakest immediately after deposition, the overburden stress

is small which makes $\overline{\Sigma}_z(t)$ large. There is a competion between the rate of loading from new snowfall and the rate of strengthening of the basal layer. The basal layer strengthens more slowly at low rates of precipitation (because σ_{zz} is smaller) but if too low, the rate of loading will not exceed the rate of strengthening.

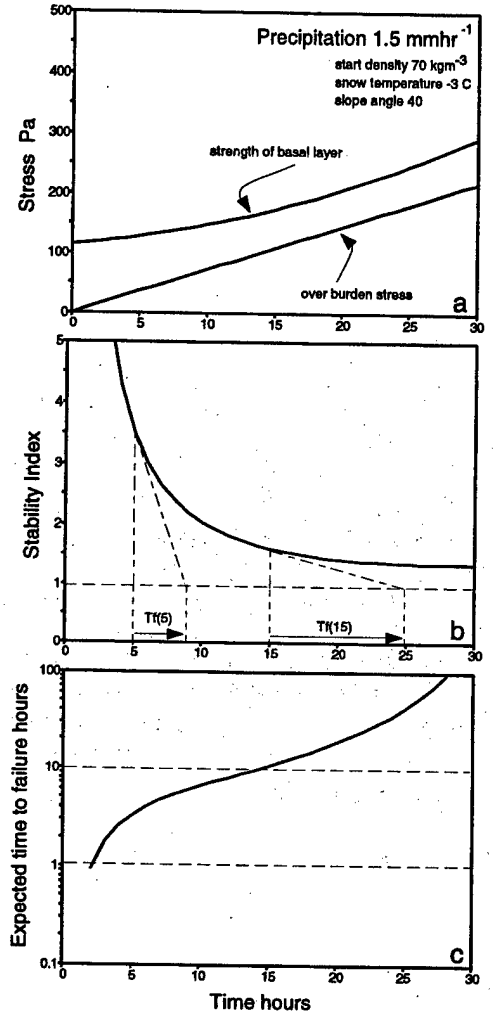

Figure 3. Evolution of stress, strength, stability index and expected time to failure calculated for constant precipitation of $1.5\,mm\,hr^{-1}$. Other initial conditions are given in the figure. In this case the model predicts stable conditions.

Fig. 3 shows the evolution of basal shear strength (initial density is $70\,kg\,m^{-3}$ and T_z is $270\,^oK$ or $-3\,^oC$) and shear stress calculated for (constant) precipitation of $1.5\,mm\,hr^{-1}$. Also shown is the stability index $\overline{\Sigma}_z(t)$ (Fig. 3b) which decreases slowly to a minimum of $\sim$ 1.3, but then increases after 35 hours (not shown). The figure also shows a graphical representation of the expected time to failure after 5 hours ($T_f(5) = 3.3\,hrs$) and after 15 hours ($T_f(15) = 10.5\,hrs$).

A continuous plot of $T_f(t)$ is shown in Fig. 3c - note the log scale. Initially $T_f(t)$ is short (Fig. 3c) but we do not expect hazardous avalanches then because the slab thickness is only $\sim 3\,cm$. $T_f(t)$ *increases* with time ($T_f(30) > 100$). The model predicts 40^o slopes will remain stable.

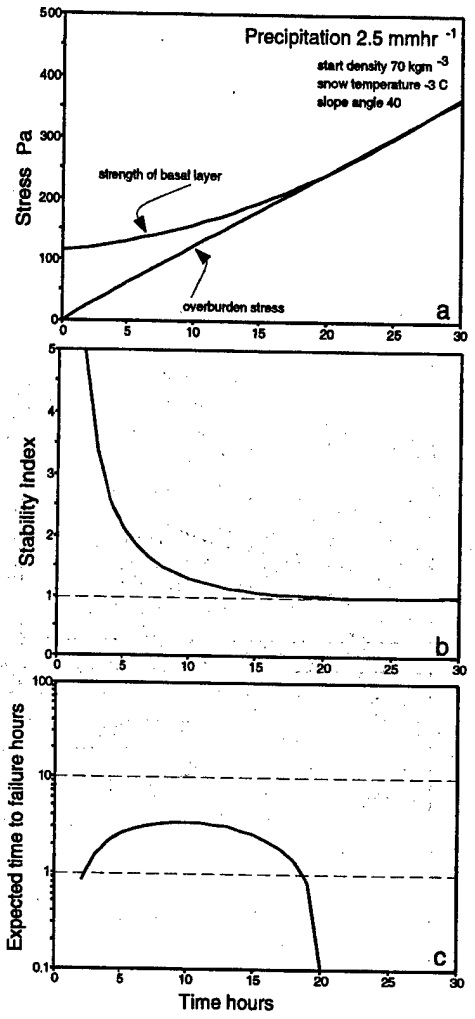

Figure 4. Evolution of stress, strength, stability index and expected time to failure calculated for (constant) precipitation of $2.5\,mm\,hr^{-1}$. Other initial conditions are given in the figure. In this case the model predicts failure after 21 hours.

Fig. 4 is a plot for constant precipitation of $2.5\,mm\,hr^{-1}$ but otherwise the same conditions as Fig. 3. $\overline{\Sigma}_z(t)$ decreases rapidly in the first 5 hours and then more slowly to a minimum value less than 1.0 after 21 hours. The expected time to failure is about 2-3 hours for the first 15 hours, but $T_f(t)$ decreases rapidly in the last 2 hours as $\overline{\Sigma}_z(t) \rightarrow 1.0$. Failure of 40^o slopes is predicted after 21 hours.

To further investigate the relationship between

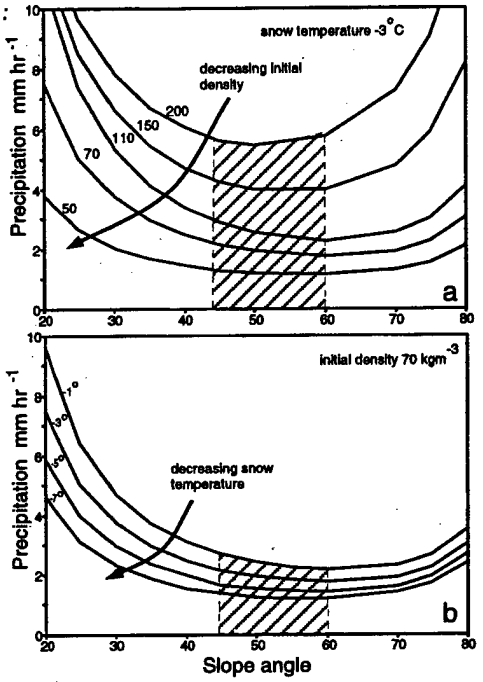

Figure 5. Critical rate of precipitation P_{wc} needed to cause $\overline{\Sigma}_z(t) < 1.0$ as a function of slope angle and the initial density of the new snow (a), and slope angle and the temperature of the new snow layer (b). The shaded areas show the range of slope angles where P_{wc} is a minimum.

precipitation rate, slope angle, initial density and temperature, we calculate the critical (constant) rate of precipitation P_{wc} needed to cause $\overline{\Sigma}_z < 1.0$. Fig.5a shows the sensitivity to slope angle and initial density (constant temperature $T_z = 270\,°K$). Fig.5b shows the sensitivity to slope angle and temperature of the basal layer (initial density $\rho_0(0) = 70\,kg\,m^{-3}$). P_{wc} is a minimum when the slope angle is somewhere between 45 and 60° (the angle depends on the initial density of the new snow). This is because for a given accumulation (measured in the earth vertical direction) the applied shear stress is a *maximum* on slopes of 45° (because $\cos\theta \sin\theta$ is a maximum when $\theta = 45°$ - Eqn.1), but the applied normal stress which directly impacts the evolving strength of the weak layer (Eqn.4) *decreases* with slope angle (because $\cos^2\theta \rightarrow 0$ as $\theta \rightarrow 90°$).

The implication is that slopes of moderate angle ($45 - 60°$) are more likely to avalanche than very steep slopes or very shallow slopes. The model also predicts avalanches are more likely when the initial snow density is low (i.e. the initial strength of the basal layer is low) and the snow temperature is cold (i.e. densification and hence strengthening of the basal layer proceeds more slowly). We note that the effective modulus E of snow increases as temperature decreases which would act to in the opposite sense to that discussed here [*McClung*, 1996].

In summary, the results indicate the probability of direct-action avalanches increases when

- the rate of precipitation is high
- the slope angle is greater than 45° but less than $\sim 60°$
- the density of the new snow is low
- the snow temperature is low

The results are no surprise to avalanche practitioners who often use such observations to estimate slope stability, but the model offers a means to quantify stability and predict when a particular slope might become unstable.

Model application - case studies

Observations of precipitation, new snow density, air temperature and avalanche activity from the Washington Cascades near Snoqualmie Pass, U.S.A. are used to test the model. The terrain near Snoqualmie Pass lies between 900 m and 1700 m. The region has a maritime climate and storms often deposit up to 1 m of new snow. Direct action avalanches are common and have a major impact on winter travellers along the Interstate 90 highway.

Measurements of new snow density at the Department of Transportation study plot (915 m a.s.l.) are used to calculate the initial strength of the new snow (Eqn. 3). A full energy balance is beyond the scope of this work and instead we assume the layer temperature is the same as the air temperature at the time of deposition. This approximation breaks down during times of rapid warming or rain when heat can be advected rapidly into the snowpack but is reasonable over short time-scales during times of snowfall. Hourly measurements of precipitation from a heated gauge either at the study plot or at a local ski area were used to calculate $\sigma_{zz}(t)$ and $\sigma_{xz}(t)$ for slopes of 40° and then used in Eqns. 4 and 5 to calculate the evolution of shear strength, shear stress, stability index, and expected time to failure.

Storm cycle of March 1, 1997

An avalanche cycle at Snoqualmie Pass on March 1, 1997 closed the I-90 highway for about 24 hours. Small slides consisting of just the recent storm snow first released early in the morning when the highway was still open. A car and a road grader were caught in a natural avalanche at the East Snowshed. No people were injured. Although the grader was

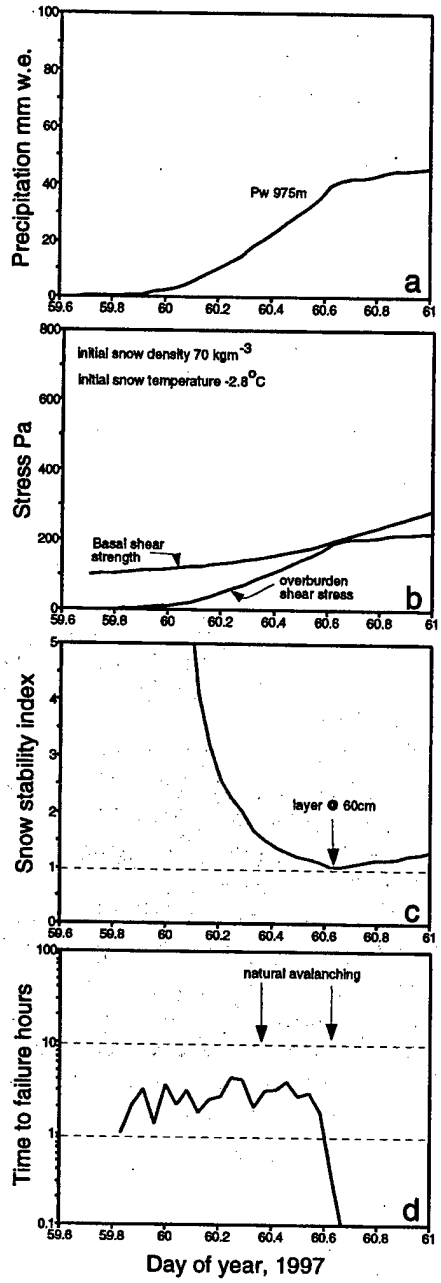

Figure 6. Measurements of cumulative precipitation at 975 m starting at 1500 hrs on February 28, 1997 (day 59.625). Also shown is the strength of the basal layer and the shear stress from the overburden for a 40° slope (b), the average stability index $\overline{\Sigma}_z(t)$ at the basal layer (c), and the expected time to failure $T_f(t)$ (d).

able to drive out of the debris, the car could not be extracted safely and it was subsequently buried by controlled avalanches. At another location a car ran into a natural avalanche crossing the highway. The vehicle was rear-ended by a following car, which was rear ended by a plow truck. A second truck veered to the side to miss the cars and ran into the avalanche. Two State Patrolmen were caught and partly buried, and 3 more cars that were backed up by the incidents were partially buried by a second avalanche. At about 1030 hrs an avalanche hit a house in the Alpental village and buried it above the third floor window. The same house and another about 100 m away was hit again at about 1500 hrs. The avalanches released from slopes above that had been recently logged. An 11 year old out of bounds skier was caught in an avalanche that swept him through trees and over a cliff. He stopped about 15 m from the highway, alive but without his equipment.

Fig. 6a shows measurements of cumulative precipitation at 975 m starting at 1500 hrs on February 28, 1997 (day 59.625). Measurements at 600 hrs on March 1 indicated 20 cm of new, low density snow ($\rho_0(0) = 70\,kg m^{-3}$, $T_s = -2.8°C$). High intensity snowfall (up to $17\,mm\,hr^{-1}$) and natural avalanche activity continued through the afternoon. Fig. 6b shows the strength of the basal layer and the shear stress from the overburden (for a 40° slope), and Fig. 6c shows the evolution of the stability index. $\overline{\Sigma}_z(t) = 1.3$ when avalanche activity first started and $\overline{\Sigma}_z(t) < 1.0$ at 1500 hrs when the basal layer was $\sim 60\,cm$ below the surface. We are not certain that the measurements in the study plot are representative of conditions in the starting zones and additional calculations indicate that if $\rho_0(0)$ was 10% lower and the local precipitation was 20% higher than measured at the study site, $\overline{\Sigma}_z(t) < 1.0$ at 1100 hrs.

Fig. 6d shows the expected time to failure varied from $\sim 2\,to\,3$ hours for most of the storm. $T_f(t)$ decreased rapidly to zero at 1500 hrs when $\overline{\Sigma}_z(t) < 1.0$.

Storm cycle of February 5, 1996

A major avalanche cycle at Snoqualmie Pass on February 5, 1996 closed the I-90 highway for 44 hours. Cars and people were caught and buried by several direct action avalanches prior to a classic warm-up and rain. One traveller who was out of his car was buried about 2 m below the surface for 29 minutes before being found by probing and dug out alive. Avalanches hit and partially buried a snow blower and a vehicle occupied by two avalanche technicians who were spotting for the blower. In all, 11 vehicles and at least 20 people were hit by avalanches; more were dusted.

Fig. 7a shows measurements of precipitation starting at noon on day 34 (February 3). By next morning 12 cm of new snow ($\rho_0(0) = 120\,kg\,m^{-3}$,

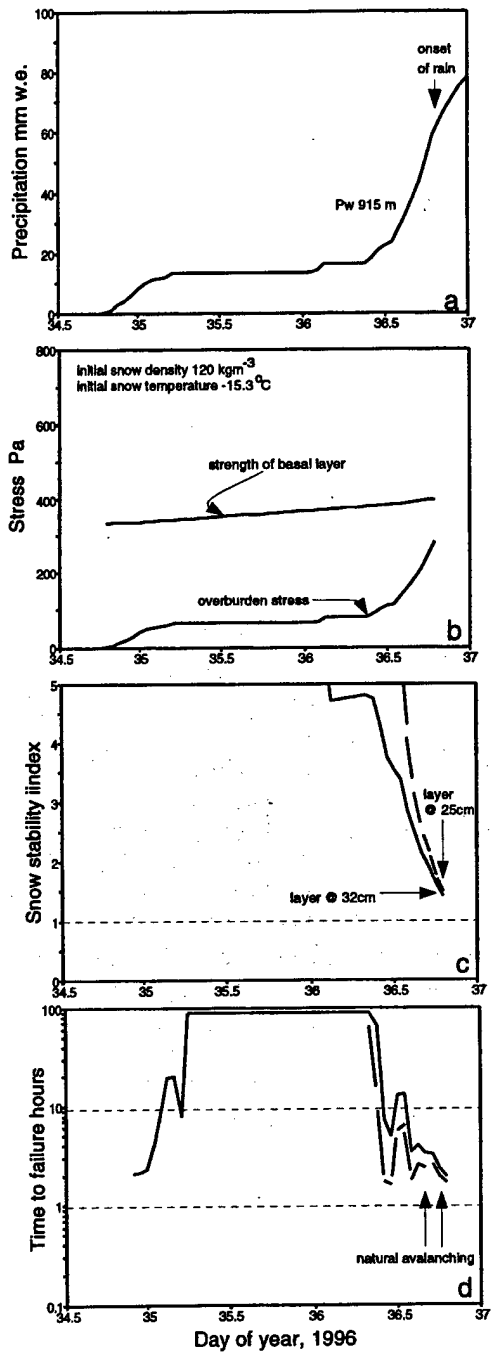

Figure 7. Measurements of cumulative precipitation at 915 m (a) starting at midday on February 3, 1996 (day 34.5). Also shown is the strength of the basal layer and the shear stress from the overburden for a 40° slope (b) the average stability index $\overline{\Sigma}_z(t)$ at two depths (c), and and the expected time to failure $T_f(t)$ at those two depths (d). Natural avalanches first ran naturally at 1730 hrs on February 5.

$T_s = -15.3°C$) had accumulated but avalanche activity was minor. The weather cleared in the afternoon but precipitation started again in the morning of day 36 (February 5). Avalanches first ran naturally at 1730 hrs, releasing as slabs about 20 cm deep. Precipitation changed to rain at 1900 hrs.

Fig. 7b shows the strength of the basal layer and the shear stress from the overburden (for a 40° slope), and Fig. 7c shows the stability index at the basal layer and at a layer deposited early in the morning of February 5 (day 36.04 - $\rho_0(0) = 110\,kg\,m^{-3}$, $T_s = -9.8°C$). $\overline{\Sigma}_z(t) = 1.6$ at the basal layer $\sim 20\,cm$ below the surface when avalanching first started. The index was higher ($\overline{\Sigma}_z(t) = 1.8$) 13 cm below the surface. However the index decreased rapidly during the evening and just prior to rain $\overline{\Sigma}_z(t) = 1.4$ both at the basal layer (then about 32 cm below the surface) and at the layer 25 cm below the surface. The measurements of snow density are surprisingly high given the cold air temperatures at the time of deposition. Other things being equal we expect new snow densities more in the range 50 to $80\,kg\,m^{-3}$ at these temperatures *LaChapelle* [1969]. It is likely that winds contributed to densify the new snow, but it is also possible that some of the new snow fell under conditions of little or no wind resulting in a buried thin, low density (weak) layer. Model calculations indicate that an initial density of $80\,kg\,m^{-3}$ (rather than $110\,kg\,m^{-3}$ measured) would cause $\overline{\Sigma}_z(t) < 1.0$ at $1700\,hrs$ - about the time of the onset of avalanching.

Fig. 7d shows the expected time to failure decreased rapidly to less than 2 hours shortly before the onset of avalanching. $T_f(t)$ remained low until rain started.

Storm cycle of January 8-15, 1989

More than 1.25 m of snow accumulated during the week of January 8-15, 1989, but no natural avalanches were observed until rain started late on January 15. Avalanche control with explosives during the storm released a few small avalanches but despite the large accumulation of snow, activity was minor. Fig. 8a shows measurements of precipitation which started as snow ($\rho_0(0) = 90\,kg\,m^{-3}$, $T_s = -0.8°C$) on January 13 and changed to rain at 1600 hrs on January 15.

Fig. 8b shows the basal shear strength and stress for a 40° slope, and Fig. 8c shows the evolution of the stability index at the basal layer and at a layer deposited early in the morning of day 14.0 ($\rho_0(0) = 95\,kg\,m^{-3}$, $T_s = -4.7°C$). The minimum stability index at the basal layer (about $40\,cm$ below the surface when rain started) was 1.7, but the minimum for the snowpack ($\overline{\Sigma}_z(t) = 1.5$) occurred $\sim 25\,cm$ below the surface just prior to rain. In this case it turns out that the stability index would *in-*

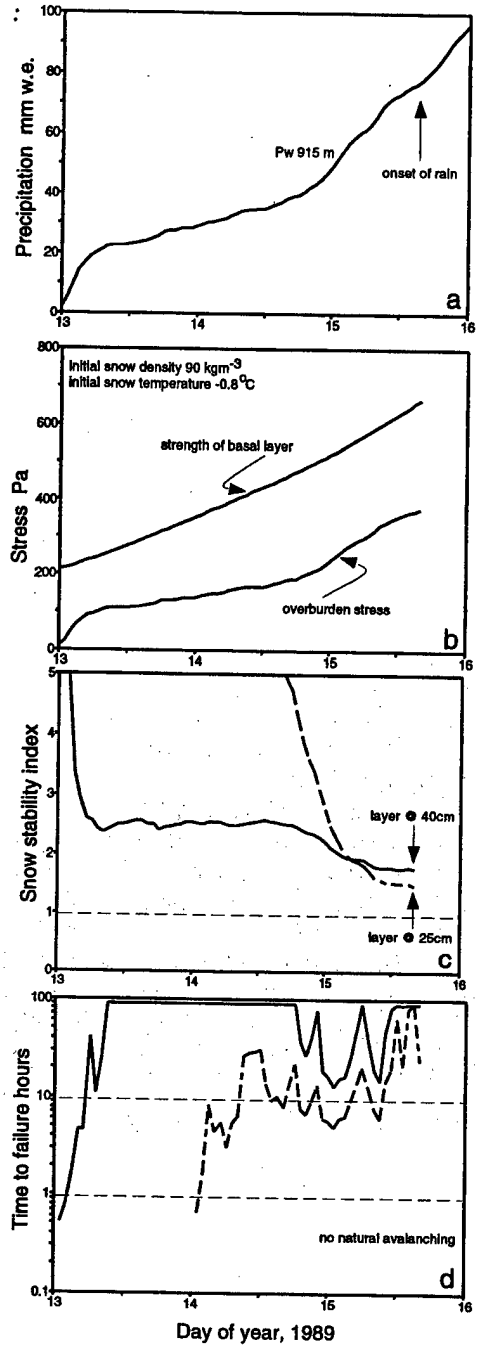

Figure 8. Measurements of cumulative precipitation at 915 m (a) starting on January 13, 1989. Also shown is the strength of the basal layer and the shear stress from the overburden for a 40° slope (b), the average stability index $\overline{\Sigma}_z(t)$ calculated at two depths (c), and the expected time to failure $T_f(t)$ at those two depths (d). Few natural avalanches released during this storm

crease for steeper slopes ($\overline{\Sigma}_z(t) = 1.6$ on slopes of 50°) but $\overline{\Sigma}_z(t) \rightarrow 1.0$ if the local precipitation was 1.75× higher than the gauge measurement or if the initial density was 65 $kg\,m^{-3}$ (rather than 95 $kg\,m^{-3}$ measured). However we do not expect such a large enhancement of precipitation, nor such a low initial density.

Fig. 8d shows the expected time to failure of both layers was generally high and *increasing* during the storm. Even when the stability index was a minimum just prior to rain, T_f was more than 30 hours. Both the magnitude and the increasing trend distinguish the T_f curve from those observed in the other two storms.

Discussion

We discussed earlier that measured values of the stability index on failed slopes are typically greater than 1.0. Several reasons might contribute to cause these apparently anomalous values of $\overline{\Sigma}_z$:

- sintering processes after failure and before testing generally act to increase the shear strength and hence measured values of Σ_z could be larger than those at the time of failure
- a shear frame test might not provide a reliable indication of strength. For example strength depends on both sample size and strain rate [*Narita*, 1983; *McClung*, 1977] and natural conditions are likely to be different from those during tests [*Sommerfeld*, 1980]
- stresses concentrate in weak or flawed regions and so the *minimum* Σ_z rather than the average might be more appropriate for assessing slope stability [*Conway*, 1998; *Conway and Abrahamson*, 1988].

If slope stability is controlled by the presence of small flaws (where $\Sigma_z < 0$) we expect instability only when the flaw exceeds some critical size [*McClung*, 1981]. That is a small flaw will not necessarily cause slope failure. Our error analysis (Sec. 2.4) does not examine flaw size explicitly, but the probability that a stability index distribution with mean $\overline{\Sigma}_z$ and uncertainty $0.65\,\Sigma_z$ will contain a value less than 1.0 can be calculated using standard methods for a single sided normal distribution. The probability $P_{\Sigma_z<1.0}$ decreases from 50% (when $\overline{\Sigma}_z = 1.0$) to 25% (when $\overline{\Sigma}_z = 1.8$).

Does the model predict instability?

Stability index We are not certain what value $\overline{\Sigma}_{zc}$ is critical for slope stability. Although encouraging that the stability index was lower during storms when avalanche activity was intense ($\overline{\Sigma}_z = 1.4$ compared to 1.5), analysis of the uncertainties and a

standard t-test indicates the two values are not significantly different.

Expected time to failure Our results suggest $T_f(t)$ discriminates much more clearly between stable and unstable conditions than $\overline{\Sigma}_z(t)$. $T_f(t)$ increased by more than an order of magnitude (from $\sim 2\,hrs$ to $> 20\,hrs$) when comparing stable and unstable conditions. This is because $T_f(t)$ contains information about both the *magnitude* and the expected *changes* of $\Sigma_z(t)$ under the current conditions. Even if $\Sigma_z(t)$ is close to critical, slopes are expected to remain stable if it is not converging to its critical value.

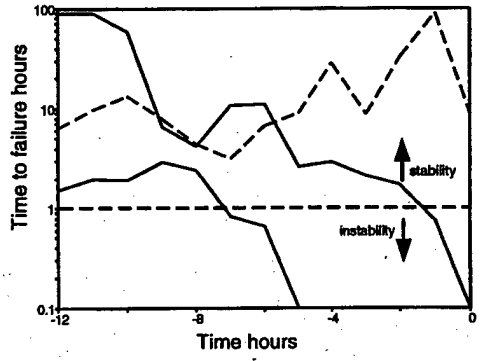

Figure 9. Expected time of failure recalculated for the three storms discussed previously assuming instability if $\overline{\Sigma}_{zc} = 1.4$.

Results suggest $T_f(t)$ discriminates much more clearly between stable and unstable conditions than $\overline{\Sigma}_z(t)$. $T_f(t)$ was more than an order of magnitude lower during storms when avalanche activity was intense ($T_f(t) = 2\,cf.\,20\,hrs$). This is because $T_f(t)$ contains information about both the *magnitude* and the expected *changes* of $\Sigma_z(t)$ under the current conditions. Even if $\Sigma_z(t)$ is close to critical, slopes are expected to remain stable if it is not converging to its critical value.

More case histories are needed to further develop and refine the model. For example results above suggest slope stability may be critical if $\overline{\Sigma}_{zc} \leq 1.4$ (rather than 1.0). Fig. 9 shows $T_f(t)$ for the three storms recalculated with $\overline{\Sigma}_{zc} = 1.4$. Using this criterion we might expect instability when $T_f(t)$ is less than $\sim 1.0\,hour$.

Model limitations

We emphasise that the model is a *tool* that may prove useful for evaluating snow slope stability during storms. Values derived from the model should be treated with caution. For example σ_f is an index of the *elastic fracture* strength - higher values are expected at lower strain rates or warmer temperatures [*McClung*, 1977, 1996]. Here we do not consider the critical strain rate condition that must also be met before failure will occur [e.g., *McClung*, 1981; *Narita*, 1983; *Gubler and Bader*, 1989; *Bader and Salm*, 1990].

We caution that the model is sensitive to the initial density of the new snow. More measurements are needed to improve the strength/density parameterization and also to improve the densification law. Although a full energy balance to model snow temperature may improve the densification law, for the short time scales of interest here, we suspect that changes in layer temperature has a small effect compared to other uncertainties. We also emphasise that the analysis is not rigorous in that we do not account for effects such as stress concentrations that would cause local stresses to be higher than the average used here, or longitudinal stresses which would act in the opposite sense providing support for the slab. Inclusion of these effects would undoubtedly improve the model but would reduce its tractability.

Model application

The simple model can be easily incorporated into a forecasting system using standard measurements of air temperature and precipitation for input. Currently the model also requires the new snow density as input but we are investigating parameterizations of new snow density using standard meteorological measurements.

Conclusions

Relatively simple parameterizations of the shear strength of buried layers and the imposed loading from the weight of the overburden offer a means to examine the evolution of snow slope stability during storms. In particular, unstable conditions are expected when the stability index $\Sigma_z(t)$ (the ratio of the shear strength of a buried weak layer at depth z to the shear stress imposed by the overburden) approaches 1.0. A related index $T_f(t)$ is the time expected to failure which takes into account both the *magnitude* and the expected *changes* of $\Sigma_z(t)$ in response to the current conditions.

Comparison of model results with measurements and observations during three storm cycles indicates $T_f(t)$ provides a particularly useful discriminator between stable and unstable conditions. Given the model assumptions and associated large uncertainties, the model does surprisingly well at predicting slope stability using standard measurements of new snow density, precipitation and air temperature.

slab release, *Cold Regions Science and Technology*, *17*, 287–300, 1990.

Bevington, P. R., and D. K. Robinson, *Data Reduction and Error Analysis for the Physical Sciences, 328pp.*, McGraw-Hill, 2nd ed., New York, 1992.

Conway, H., The impact of surface perturbations on snow-slope stability, *Ann. Glaciol.*, *26*, 307–312, 1998.

Conway, H., and J. A. Abrahamson, Snowslope stability - a probabilistic approach, *J. Glaciol.*, *34*(117), 170–177, 1988.

Fohn, P. M. B., The Rutschlock as a practical tool for slope stability evaluation, in *Avalanche Movement and Effects. Proc., Davos Symposium*, no. 162, pp. 223–228, Int. Ass. Hydrol. Sci., 1987.

Gibson, L. J., and M. F. Ashby, *Cellular solids. Structure and properties*, Pergamon Press, New York, 1987, 336 pp.

Gubler, H., and H.-P. Bader, A model of initial failure in slab-avalanche release, *Ann. Glaciol.*, *13*, 90–95, 1989.

Hansen, A. C., and R. L. Brown, A new constitutive theory for snow based on a micro-mechanical approach, in *Avalanche Movement and Effects. Proc. Davos Symposium*, no. 162, pp. 87–104, Int. Ass. Hydrol. Sci., 1987.

Jamieson, J. B., Avalanche prediction for persistent snow slabs, Ph.D. thesis, Dept. Civil Eng., Univ. Calgary, Alberta, Canada, 1995, 258pp.

Jamieson, J. B., and C. D. Johnson, Rutschblock precision, technique variations and limitations, *J. Glaciol.*, *39*(133), 666–674, 1993a.

Jamieson, J. B., and C. D. Johnson, Shear frame stability parameters for large scale avalanche forecasting, *Ann. Glaciol.*, *18*, 268–273, 1993b.

Keeler, C. M., The growth of bonds and the increase of mechanical strength in a dry seasonal snow-pack, *J. Glaciol.*, *8*(54), 441–450, 1969.

Kojima, K., Densification of seasonal snowcover, in *Physics of Snow and Ice, Proc. Int. Conf. on Low Temp. Sci.*, edited by H. Oura, vol. 1, pp. 929–952, Hokkaido Univ., Sapporo, 1967.

LaChapelle, E. R., Properties of snow. Paper prepared for Hydrologic Systems course presented by College of Forest Resources, University of Washington, Seattle, 21pp., 1969.

Marshall, H. P., H. Conway, and L. A. Rasmussen, Snow densification during rain, *Cold Regions Science and Technology*, submitted.

McClung, D. M., Direct simple shear stress tests on snow and their relation to slab avalanche formation, *J. Glaciol.*, *19*(81), 101–109, 1977.

McClung, D. M., Fracture mechanical models of dry slab avalanche release, *J. Geophys. Res.*, *86*, 10783–10790, 1981.

McClung, D. M., Effects of temperature on fracture in dry slab avalanche release, *J. Geophys. Res.*, *101*, 21907–21920, 1996.

271pp.

Narita, H., An experimental study on tensile fracture of snow, *Low Temp. Science, Ser. A*, *32*, 1–37, 1983.

Perla, R., Slab avalanche measurements, *Can. Geotech. J.*, *14*(2), 206–213, 1977.

Perla, R., and E. LaChapelle, A theory of snow slab failure, *J. Geophys. Res.*, *75*(36), 7619–7627, 1970.

Perla, R., T. Beck, and T. Cheng, The shear strength index of alpine snow, *Cold Regions Science and Technology*, *6*(1), 1982.

Roch, A., Les variations de la resistance de la neige, *Int. Ass. Hydrol. Sci.*, *69*, 86–99, 1966.

Schaerer, P., Evaluation of the shovel shear test, in *Proceedings Int. Snow Sci. Workshop, Whistler, BC*, pp. 274–276, 1989.

Sommerfeld, R., Statistical models of snow strength, *J. Glaciol.*, *26*(94), 1980.

Sommerfeld, R., and R. M. King, A recommendation for the application of the Roch index for slab avalanche release, *J. Glaciol.*, *22*(88), 1979.

H. Conway, Geophysics Box 351650, U. of Washington, Seattle, WA 98195, conway@geophys.washington.edu, and C. Wilbour, Box 141, Snoqualmie Pass, WA 98068.

This preprint was prepared with AGU's LaTeX macros v4, with the extension package 'AGU++' by P. W. Daly, version 1.5d from 1997/04/28.

Acknowledgments

This research was funded by the U.S. Army Research Office (Grant No. DAAH04-95-1-0172). We also wish to thank the Washington State Department of Transportation for logistical support and Al Rasmussen for his assistance.